



Individual tree point clouds and tree measurements from multi-platform laser scanning in German forests

Hannah Weiser¹, Jannika Schäfer², Lukas Winiwarter¹, Nina Krašovec^{1,3}, Fabian E. Fassnacht^{2,4}, and Bernhard Höfle^{1,5}

¹3DGeo Research Group, Institute of Geography, Heidelberg University, Heidelberg, Germany

²Institute of Geography and Geoecology, Karlsruhe Institute of Technology, Karlsruhe, Germany

³Department of Psychiatry and Psychotherapy, Central Institute of Mental Health,
Medical Faculty Mannheim, Heidelberg University, Mannheim, Germany

⁴Remote Sensing and Geoinformatics, Freie Universität Berlin, Berlin, Germany

⁵Interdisciplinary Center for Scientific Computing (IWR), Heidelberg University, Heidelberg, Germany

Correspondence: Hannah Weiser (h.weiser@uni-heidelberg.de)

Received: 28 January 2022 – Discussion started: 4 February 2022

Revised: 10 June 2022 – Accepted: 13 June 2022 – Published: 5 July 2022

Abstract. Laser scanning from different acquisition platforms enables the collection of 3D point clouds from different perspectives and with varying resolutions. These point clouds allow us to retrieve detailed information on the individual tree and forest structure. We conducted airborne laser scanning (ALS), uncrewed aerial vehicle (UAV)-borne laser scanning (ULS) and terrestrial laser scanning (TLS) in two German mixed forests with species typical of central Europe. We provide the spatially overlapping, georeferenced point clouds for 12 forest plots. As a result of individual tree extraction, we furthermore present a comprehensive database of tree point clouds and corresponding tree metrics. Tree metrics were derived from the point clouds and, for half of the plots, also measured in the field. Our dataset may be used for the creation of 3D tree models for radiative transfer modeling or lidar simulation studies or to fit allometric equations between point cloud metrics and forest inventory variables. It can further serve as a benchmark dataset for different algorithms and machine learning tasks, in particular automated individual tree segmentation, tree species classification or forest inventory metric prediction. The dataset and supplementary metadata are available for download, hosted by the PANGAEA data publisher at <https://doi.org/10.1594/PANGAEA.942856> (Weiser et al., 2022a).

1 Introduction

Airborne and terrestrial laser scanning enables the collection of detailed 3D information on forest structure. This information can be used to estimate important tree and stand height (Pearse et al., 2019; Wang et al., 2019), wood volume (Dassot et al., 2012; Disney et al., 2018), biomass (Disney et al., 2018; Næsset et al., 2011), canopy cover (Arumäe and Lang, 2018; Smith et al., 2009), tree density (Pearse et al., 2019), diameter at breast height (DBH) (Bruggisser et al., 2020; Liu et al., 2018) and basal area (Pearse et al., 2019). Laser scanning data from airplanes and helicopters have been widely applied in the for-

est sector and are operationally used for forest inventories in several countries (Montaghi et al., 2013; Scion, 2021; White et al., 2017) using the area-based approach (Bouvier et al., 2015; Holopainen et al., 2014; Næsset, 2002). In the area-based approach, wall-to-wall laser scanning data are combined with information collected in field plots to estimate forest attributes across the complete area covered by the laser scanning survey. Besides the area-based approach, individual tree-based approaches in which first single trees are detected from the point clouds and then attributes are estimated for the individual trees have also received attention (Latifi et al., 2015; Maltamo et al., 2004). Terrestrial laser scanning data with stationary or mobile sensors can be used to

obtain detailed information on individual trees which typically cannot be directly derived from airborne surveys. Corresponding attributes include DBH and tree stem taper information but also information on small-scale understory variation which may be important for characterizing local fuel conditions or habitat properties. Finally, laser scanning with uncrewed aerial vehicles (UAVs) represents a compromise between airborne and terrestrial laser scanning. UAV-borne laser scanning (ULS) allows for data collection over larger areas compared to TLS but cannot reach the fine spatial resolution of TLS data. Due to the lower flying height, ULS achieves higher point densities and a better penetration of the canopy than ALS but covers smaller areas due to constraints in flying time and speed.

Over the last years, notable progress has been made in both sensor systems and workflows to derive forest attributes from laser scanning data collected by various platforms (Calders et al., 2020; Maltamo et al., 2014; Morsdorf et al., 2017; Roussel et al., 2020; Wallace et al., 2014). At the same time, there is still space for improvements, for example, when it comes to (1) understanding and comparing the potential of tree delineation algorithms or (2) deriving certain attributes such as tree species from laser scanning point clouds. Furthermore, (3) there are still open questions related to the influence of acquisition settings on the model performances in the area-based approach. For issues (1) and (2), obtaining reliable reference data in the field is often extremely challenging and time-intensive, and preparing openly available high-quality benchmark datasets may contribute to making further advancement in the research field. For issue (3), cost is often a limiting factor since in many cases it is impossible to acquire numerous ALS flights in a research project to examine the influence of acquisition parameters due to the high costs of the flights. In this case, a combination of synthetic forest stands and laser scanning simulators may be one way forward by enabling extensive sensitivity analyses (Disney et al., 2010; Roberts et al., 2020).

One key element for creating synthetic forest stands, enabling laser scanning simulations, is detailed and realistic 3D tree models, which can be reconstructed from 3D point clouds obtained with terrestrial, UAV-borne or airborne laser scanning. Virtual forest scenes can be built from such 3D tree models and used as input to complex radiative transfer models (e.g., DART; Gastellu-Etchegorry et al., 2015) or light detection and ranging (lidar) simulators (e.g., HE-LIOS++; Winiwarter et al., 2022). Such simulations enable an improved understanding of the relation between forests' structural elements and electromagnetic radiation (Disney et al., 2010; Weiser et al., 2021; Widlowski et al., 2015). This is particularly relevant for improving remote-sensing-assisted forest inventory approaches. Three-dimensional tree models derived from laser scans of real trees have also been used to develop structural tree allometries to, e.g., non-destructively estimate the above-ground biomass of tree individuals (Calders et al., 2015). Further, 3D tree models can

be used to parameterize ecophysiological models (Sinoquet et al., 2001) to quantify shading effects and evapotranspiration properties of urban trees. Other applications of detailed tree models include their integration in 3D visualizations as, e.g., used in urban landscape planning projects or in computer games (Bournez et al., 2017).

(Semi-)automated methods to extract tree models from TLS point clouds are readily available (e.g., SimpleTree/SimpleForest, Hackenberg et al., 2015; TreeQSM, Rauomonen et al., 2013), but data collection and extraction of high-quality tree point clouds is still very time-consuming because it requires manual interaction and control. This generally limits the acquisition and processing of very large numbers of trees in single projects and thus underlines the importance of publishing such datasets as open data for shared usage.

The dataset presented here is one of the biggest open-access collections of multi-platform tree point clouds with matching inventory data of common tree species of central European forests. We present 1491 trees which were identified in point clouds acquired in 12 forest plots in southwest Germany. A total of 249 trees were extracted from all three types of point clouds, ALS, ULS and TLS. Another 1031 trees were extracted from both ALS and ULS point clouds. A total of 1168 trees were extracted from two different ULS datasets, acquired under leaf-on conditions and leaf-off conditions (Fig. 8). The maximum time period between laser scanning acquisitions under leaf-on conditions is 70 d. Single tree metrics, including species, height, DBH and crown metrics, were derived from the point clouds and, for half of the plots (1060 trees), also measured in the field. Thus, one or more point clouds and corresponding metrics are provided for each tree. In addition to the 3D coordinates, each point of the point cloud has attributes including reflectance, echo number, waveform deviation and time of recording. The dataset further exists of the larger area forest point clouds of the acquisitions and the flight trajectory or scan position information.

Figure 1 displays the workflow of the data acquisition and processing steps.

2 Methods

In this section, we introduce the study site, give an overview of the measurements taken in the field and document the lidar acquisitions from the three different platforms (airborne, UAV-borne and terrestrial) which were conducted in 2019 and 2020 under leaf-on and leaf-off canopy conditions. We describe how we extracted single-tree point clouds from the lidar datasets to (a) match them to the field measurements and (b) derive individual tree metrics directly from the point clouds.

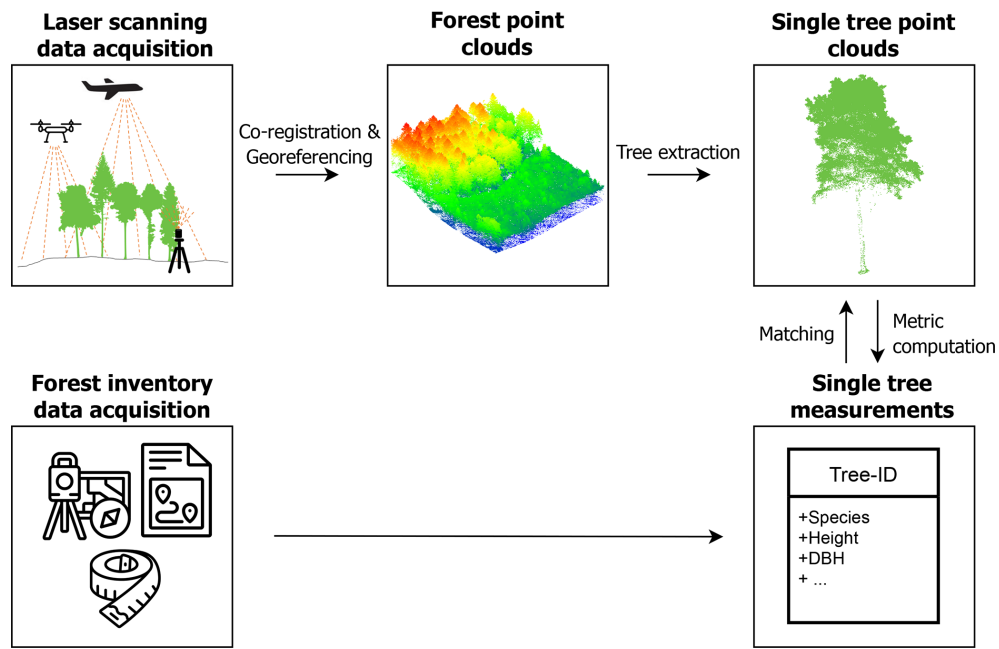


Figure 1. Workflow for the generation of the dataset, starting with the laser scanning data acquisition and forest inventory measurements and resulting in single-tree point clouds and corresponding point-cloud-derived and field-measured metrics. This figure has been designed using resources from <http://www.flaticon.com/> (last access: 3 August 2021; Smashicons, Freepik).

2.1 Study site

The two study sites, the Bretten municipal forest ($49^{\circ}00'36''$ N, $8^{\circ}41'35''$ E) and the Hardtwald forest in Karlsruhe-Waldstadt ($49^{\circ}02'04''$ N, $8^{\circ}25'40''$ E), are located in a region of temperate forests in the federal state of Baden-Württemberg, Germany. Data acquisitions cover three forest plots in the Karlsruhe forest and nine in the Bretten municipal forest, totaling 12 forest plots (Fig. 2). The Bretten site is characterized by the hilly landscape of the Kraichgau, and the Karlsruhe site is on flat terrain of the Upper Rhine Plain. The main tree species in the managed forest stands are Scots pine (*Pinus sylvestris* L.), European beech (*Fagus sylvatica* L.), common oak (*Quercus robur* L.), sessile oak (*Quercus petraea* (Matt.) Liebl.), red oak (*Quercus rubra* L.), European hornbeam (*Carpinus betulus* L.), Douglas fir (*Pseudotsuga menziesii* (Mirb.) Franco) and Norway spruce (*Picea abies* (L.) H. Karst.). Most stands have multiple layers, a mixed species composition and a dense forest cover. Karlsruhe plots are dominated by Scots pine, red oak and beech. Bretten plots are more diverse and characterized by beech, spruce, Douglas fir, oaks (mostly sessile oak) and European hornbeam. We provide a summary of forest plot characteristics in Table A1 in the Appendix, including the number of trees, basal area ($\text{m}^2 \text{ha}^{-1}$), the percentage of dead trees and the median tree height (m), also separated by tree species.

2.2 Laser scanning data acquisition and co-registration of the multi-modal datasets

2.2.1 Airborne laser scanning (ALS)

MILAN Geoservice GmbH was commissioned by the Institute of Geography and Geoecology (IFGG) of Karlsruhe Institute of Technology (KIT) to carry out the ALS acquisitions. The flights were conducted on 5 July 2019 under leaf-on conditions with a *RIEGL VQ-780i* (*RIEGL* Laser Measurement Systems, 2019) sensor mounted on an aircraft of type Cessna C207. Data were acquired in 38 parallel flight strips, plus two orthogonal strips, in Karlsruhe, covering an area of around 65 km^2 . In Bretten, data were acquired in 25 parallel flight strips, plus two orthogonal strips, covering an area of around 32 km^2 . Detailed sensor and acquisition parameters are listed in Table 1. The data were georeferenced and transformed into the coordinate reference system ETRS89/UTM zone 32 (EPSG:25832) with ellipsoidal height (GRS80). Full-waveform data are available from the authors on reasonable request.

For quality control, seven small built-up areas surrounding the area of interest were recorded by the 3DGeo Research Group of Heidelberg University using ULS, for which georeferencing was carried out as described in the next section.

Flight strips were merged and the point clouds were clipped to the 12 forest plots, using a generously sized buffer to cover the other datasets (ULS, TLS and field measurements). This resulted in extracted ALS point clouds of $300 \text{ m} \times 300 \text{ m}$, $200 \text{ m} \times 200 \text{ m}$ or $140 \text{ m} \times 140 \text{ m}$ extent

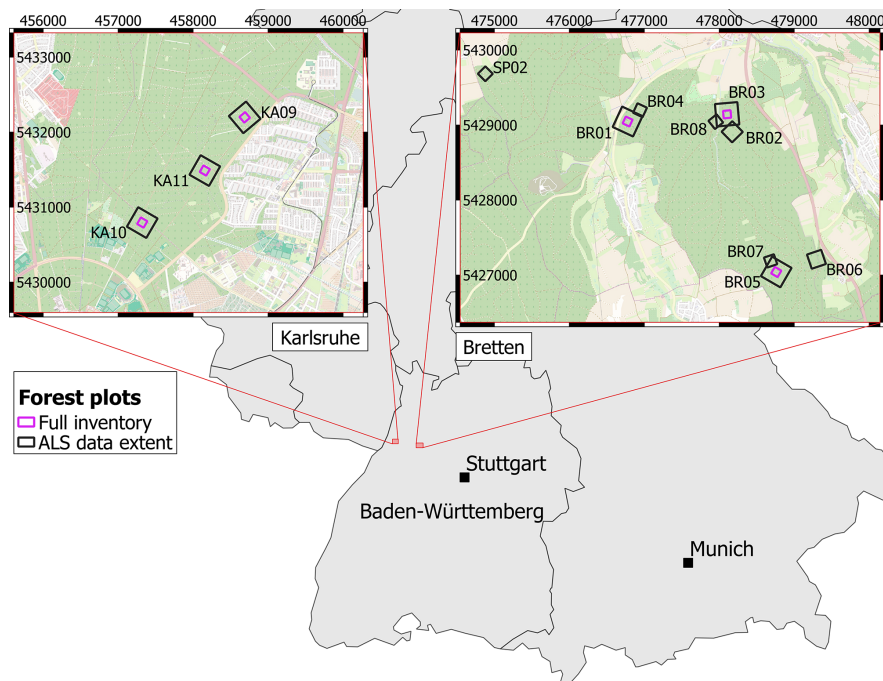


Figure 2. Map of the forest plots in Karlsruhe (left) and Bretten (right) in the federal state of Baden-Württemberg, Germany. The extent of the extracted ALS data is outlined in black, and areas for which field measurements were conducted are outlined in purple (“Full inventory”). All plots except BR04 are covered by the ULS acquisitions. TLS was performed in selected locations within the plots. Coordinates are given in the projected coordinate system ETRS89/UTM zone 32N (EPSG:25832). Map data: © OpenStreetMap contributors 2021. Distributed under the Open Data Commons Open Database License (ODbL) v1.0. Administrative boundaries: © EuroGeographics (2021).

(Fig. 2), depending on the spatial coverage of the TLS and ULS datasets. Pulse density grids with a cell size of 1 m were computed for each point cloud. Pulse density, averaged over all 12 plot point clouds, was 72.5 pts m^{-2} (standard deviation: 31.0 pts m^{-2}).

2.2.2 UAV-borne laser scanning (ULS)

UAV-borne laser scanning point clouds were acquired with a *RIEGL* miniVUX-1UAV (*RIEGL* Laser Measurement Systems, 2020c) sensor mounted on a DJI Matrice 600 Pro hexacopter (DJI, 2018). Flights were conducted in August and September 2019, in December 2019, and in March and April 2020 to obtain data of trees under both leaf-on and leaf-off conditions. Table 1 shows the general settings used in all 21 flights. For plots KA10 and KA11 in Karlsruhe, only leaf-on data were acquired in summer. Two overlapping double grid patterns, offset by 45° in orientation, were employed for all flights (Fig. 3). In the 2019 flights, adaptive banked turns were flown, while in the 2020 flights, the UAV was operated in stop and turn mode, i.e., stopped in each corner to turn without inclining about the roll axis. Flying altitude, speed, scan frequency, and flight line distance varied across the different flight campaigns and are listed in Table 2. Note that for the 2019 flights of plots BR03 and BR08, the two parts of the double cross were flown at different speeds.

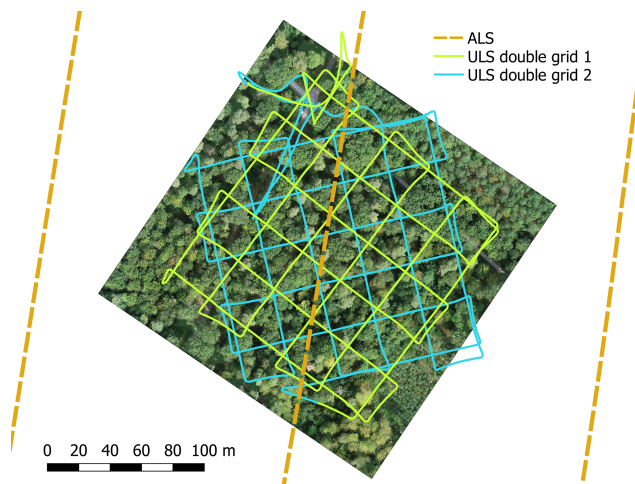


Figure 3. UAV-borne laser scanning (ULS) and airborne laser scanning (ALS) flight trajectories of plot KA10. Background: orthophoto of the forest plot, acquired on 6 September 2019.

ULS data were processed using the software RiPROCESS (*RIEGL* Laser Measurement Systems, 2020a, version 1.4.2). GNSS reference measurements were retrieved as a virtual base station from SAPOS Baden-Württemberg (<https://www.sapos-bw.de>, last access: 6 May 2020) and were used to post-

Table 1. Airborne laser scanning (ALS), UAV-borne laser scanning (ULS) and terrestrial laser scanning (TLS) sensor and acquisition parameters. Sensor specifications are according to the data sheets (*RIEGL* Laser Measurement Systems, 2017, 2019, 2020c).

Mode	ALS
Aircraft	Cessna C207
Sensor	<i>RIEGL</i> VQ-780i
Laser beam divergence	0.25 mrad (measured at the $1/e^2$ points)
Pulse repetition frequency	1000 kHz
Scan frequency	225 lines per second
Altitude above ground	650 m
Off-nadir scan angle	$\pm 30^\circ$
Flight line distance	175 m
Flight line overlap	76 %
Speed	100 kn ($\approx 51.4 \text{ m s}^{-1}$)
Date	5 July 2019
Mode	ULS
UAV	DJI Matrice 600 Pro
Sensor	<i>RIEGL</i> miniVUX-1UAV
Laser beam divergence	$\approx 2.72 \text{ mrad} \times 0.85 \text{ mrad}$ (measured at the $1/e^2$ points; $1.6 \text{ mrad} \times 0.5 \text{ mrad}$ measured at 50 % peak intensity)
Pulse repetition frequency	100 kHz
Off-nadir scan angle	$\pm 90^\circ$
Mode	TLS
Sensor	<i>RIEGL</i> VZ-400
Laser beam divergence	0.3 mrad (measured at the $1/e^2$ points)
Pulse repetition frequency	300 kHz
Scan angle range	100° (-40 to $+60^\circ$ from the horizontal plane)

process the trajectory using Applanix PosPac MMS (Applanix Corporation, 2018, version 8.3). The trajectory and the point cloud data from the scanner were imported to RiPROCESS. At import, the point cloud data were filtered for reflectance between -22 and $+10$ dB, scan angle $\leq \pm 90^\circ$ off nadir, and ranges between 5 and 150 m to filter outliers from the data. The point cloud data were converted from the scanner (SDCImport) and then transformed from local polar to world coordinates (ETRS89/UTM Zone 32N) using the flight trajectory (RiWORLD). For the subsequent strip adjustment, only points with a scan angle $\leq \pm 45^\circ$ off nadir were considered because larger off-nadir angles constitute almost only within-canopy returns, which we presumed to be less accurate and/or less suitable for strip adjustment. Finally, each flight strip (with the full scan angle range of $\pm 90^\circ$) was exported in LAZ format including intensity information (signal amplitude and reflectance) and waveform information (pulse shape deviation). Using LAStools (Rapidlasso GmbH, 2020, version 200509), the single flight strips were merged, and the information on the flight lines was encoded in the LAS field “Point Source ID”.

Pulse density grids were computed for extracted 1 ha point clouds of the 12 plots (i.e., excluding the edges of the flight lines) with a cell size of 1 m. The mean pulse densities derived for these grids are shown in Table 2.

2.2.3 Terrestrial laser scanning (TLS)

TLS acquisitions were performed at selected spots within the 12 forest plots. Our focus was on the most common species in our study site. In total, we conducted 31 TLS surveys on 20 d between June and September 2019 under leaf-on conditions. In each survey, a group of selected trees was scanned from five to eight scan positions (SPs), regularly distributed around the target trees. Depending on the size of the scan area, the terrain and the forest density, the number and the exact positions of the SPs were adjusted. The scans were acquired with a *RIEGL* VZ-400 terrestrial laser scanner, which has a wavelength of 1550 nm and a beam divergence of 0.3 mrad (full angle, measured at the $1/e^2$ points; *RIEGL* Laser Measurement Systems, 2017, Table 1). Scans were performed with a pulse repetition frequency (PRF) of 300 kHz and vertical and horizontal angle increments of 0.017° (0.3 mrad). This results in 3 mm point spacing at 10 m range for a single scan and ensures non-overlapping footprints. Only in three acquisitions on 3 and 4 June 2019 was the vertical resolution erroneously set to 0.099° (1.73 mrad). Each scan had a vertical field of view of 100° (-40 to $+60^\circ$ from the horizontal plane) and a horizontal field of view of 60 to 100° facing the target trees. If the distance between scanner and target trees was low in relation to the tree height, we performed an additional tilted scan at respective SPs to increase the vertical extent of the scan.

Table 2. UAV-borne laser scanning acquisition parameters per flight and resulting approximate pulse densities, quantified on extracted point clouds of 1 ha, thereby excluding points on the flight line edges. For altitude above ground, a mean value is given, with the standard deviation in parentheses.

Plot	Date (yyyy-mm-dd)	Canopy condition	Scan frequency [lines s ⁻¹]	Altitude above ground [m]	Speed [m s ⁻¹]	Flight line distance [m]	Mean pulse density [pts m ⁻²]
BR01	2019-09-12	leaf-on	33.4	68.3 (2.4)	5.0	30	936
	2019-12-04	leaf-off	33.0	62.3 (1.7)	5.0	30	859
	2020-03-27	leaf-off	33.4	72.4 (1.9)	5.0	27	824
BR02	2019-08-24	leaf-on	100	72.1 (3.4)	5.0	26	1091
	2020-04-01	leaf-off	33.4	62.4 (3.9)	5.0	26	1026
BR03	2019-08-24	leaf-on	100	62.5 (1.3)	5.0/4.0	26	1262
	2020-03-31	leaf-off	33.4	67.7 (2.9)	5.0	27	1114
BR05	2019-09-12	leaf-on	33.4	70.8 (4.7)	5.0	30	909
	2020-03-26	leaf-off	33.4	74.5 (5.0)	5.0	27	988
BR06	2019-09-12	leaf-on	33.4	61.2 (2.8)	5.0	30	953
	2020-03-27	leaf-off	33.4	61.2 (3.3)	5.0	26	1023
BR07	2019-08-24	leaf-on	100	70.1 (5.7)	4.4	26	1115
	2020-03-26	leaf-off	33.4	71.4 (5.4)	5.0	27	1050
BR08	2019-08-24	leaf-on	100	63.9 (2.2)	5.0/4.0	26	1205
	2020-03-31	leaf-off	33.4	69.3 (2.3)	5.0	27	1024
SP02	2019-09-03	leaf-on	100	64.0 (2.5)	4.0	25	797
	2020-04-01	leaf-off	33.4	66.2 (3.1)	5.0	26	919
KA09	2019-09-13	leaf-on	33.4	65.6 (0.8)	5.0	30	941
	2019-12-10	leaf-off	33.4	60.9 (0.8)	5.0	30	987
KA10	2019-09-13	leaf-on	33.4	64.9 (0.8)	4.8	30	1036
KA11	2019-09-06	leaf-on	33.4	64.4 (1.0)	3.0	25	1554

Five cylindrical reflective targets mounted on tripods were positioned in the area to be scanned. They serve as tie points in the tie-point-based co-registration of multiple scans. Further circular reflectors were pinned onto trees of interest to later facilitate their identification in the point cloud.

For each campaign, RTK GNSS measurements from one scan position, referred to as the *main stable position*, and one tie point were used for initial georeferencing of the respective scan. Remaining scans were registered to the main stable position in the software RiSCAN PRO (RIEGL Laser Measurement Systems, 2020b, versions 2.8.0, 2.8.2, 2.9.0) using the cylindrical and circular reflective targets in the scene. After the tie-point-based registration, a fine alignment was performed using the Multi Station Adjustment (MSA) function of RiSCAN PRO, which uses a variant of the iterative closest point (ICP) algorithm based on planar areas in the point cloud. Because of the weak GNSS signal below the leaf canopy, the positional measurements taken in the forest only allowed for coarse georeferencing of the TLS point clouds. Therefore, TLS point clouds were registered to the ULS point clouds by tree matching and subsequent ICP-alignment. Be-

cause stems are sampled better in the leaf-off point clouds due to the higher penetrability of the defoliated crowns, we used the ULS leaf-off point clouds for stem detection where available. TLS point clouds were downsampled for the stem detection using the RiSCAN PRO octree filter with a voxel size of 0.05 m. We calculated normal vectors, linearity and 3D point densities in corresponding TLS and ULS point clouds using OPALS (Pfeifer et al., 2014, version 2.3.1). By filtering for these three attributes, stem points were extracted and then segmented. To derive the final stem positions, each segment was projected to the horizontal plane and the center of gravity was computed. For each pair of overlapping point clouds, TLS-derived tree positions were manually matched to ULS-derived tree positions, and the resulting rigid transformation was applied to the TLS point cloud. The height offset was estimated by selecting corresponding points in a vertical profile in both point clouds. After correcting the height offset, a fine alignment between TLS and ULS point clouds was performed with the ICP implementation of OPALS. A visual assessment of the alignment between ALS, ULS and TLS is presented in Fig. 4.

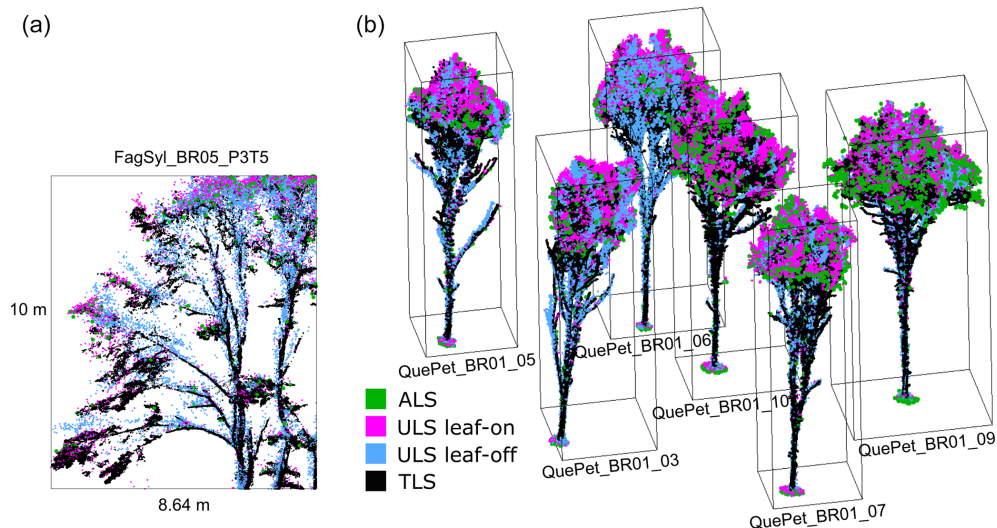


Figure 4. Point cloud visualizations showing the different point density and coverage for each platform. **(a)** Section of point clouds of a beech tree in plot BR05. The section has a depth of 1 m. **(b)** Point clouds of oaks in plot BR01. The trees are 16 to 18 m tall. Point clouds are labeled by their tree ID in the dataset.

2.3 Tree point cloud extraction

We used different procedures to extract single-tree point clouds from the laser scanning data (Fig. 5). The full TLS point clouds were automatically segmented into individual tree point clouds (Sect. 2.3.1). For the trees of interest in the center of the acquired scene, the segmentation was improved by manual editing. ULS and ALS tree point clouds were delineated manually in the point clouds. Because our multi-platform laser scanning point clouds are georeferenced and spatially overlapping, it was possible to extract trees from one point cloud using tree point clouds already extracted from another platform or acquisition. This way, we only had to delineate each tree in one of the overlapping point clouds. Table 5 and Fig. 8 give an overview of the number of tree point clouds that are available for each data source, i.e., for each platform and canopy condition.

2.3.1 Automatic tree segmentation from TLS point clouds and manual post-processing

A total of 264 trees were extracted from the TLS point clouds. We first automatically segmented each TLS plot and then refined the segmentation result for our selected trees by manually editing the point clouds.

Automatic segmentation was performed with Computree software (Computree Group, 2022, version 5.0.054b). The workflow consists of an Euclidean clustering approach combined with a competitive Dijkstra algorithm and relies largely on the SimpleTree plugin (Hackenberg, 2017, Beta version 4.33.06). After importing the point cloud of the forest scene, a digital terrain model (DTM) is computed. Next, a slice of the point cloud is extracted between 1.0 and 1.6 m

above the DTM. The sliced point cloud is spatially clustered to derive one seed cluster per tree stem. Each point in a stem seed is assigned a cluster ID and an initial distance of 0. A competitive Dijkstra algorithm is run, where each vegetation point is connected to one of the clusters and receives the according cluster ID. A graph is built from the connected points. If there are multiple possible paths between a seed point and a target point, the shortest path is chosen.

The result of this automatic approach is error-prone, i.e., Dijkstra's algorithm cannot guarantee the assignment of each point to the correct tree cluster. This is due to overlapping tree crowns and occlusions in the crown. Furthermore, errors in the clustering of stems seeds can lead to false labeling of points.

We applied a manual correction procedure. Selected tree point clouds were compared to surrounding segmented trees to identify erroneous or missing points and correct them manually. This was done in two stages by independent editors using the interactive segmentation tool of CloudCompare (CloudCompare, 2019, version 2.10.2). Human experts can take into account the morphology of the crowns in ways which are barely feasible automatically. A combined approach of automatic segmentation and manual correction is therefore a good solution to precisely delineate trees.

2.3.2 Manual tree extraction from ALS and ULS point clouds

From ALS and ULS point clouds, we delineated trees manually in the point cloud using the interactive segmentation tool of CloudCompare, or we used already manually delineated trees as templates for automatic extraction (Sect. 2.3.3).

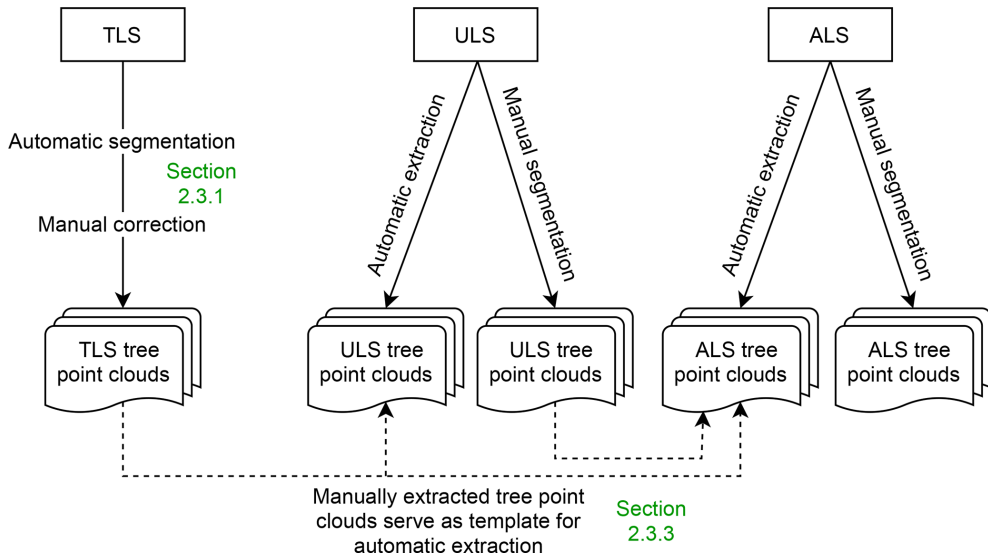


Figure 5. The different ways of single tree extraction. TLS point clouds were extracted with a combination of automatic segmentation and manual correction. ULS and ALS point clouds were partly segmented manually and partly extracted using a higher-resolution point cloud from another platform (i.e., TLS and ULS).

2.3.3 Automatic tree extraction from ALS and ULS point clouds using extracted template tree point clouds

Because our laser scanning point clouds are spatially overlapping and co-registered, we were able to use tree point clouds already extracted from one dataset to query points from another dataset. For each point in the source tree point cloud, we queried all nearest neighbors within a given search radius in the larger area target point cloud to extract the same tree in the target point cloud. This was done with a k -nearest-neighbor (k NN) search using a k -d tree. We ensured that the source point clouds were of equal resolution or higher resolution than the target point clouds to avoid extrapolation. For instance, we extracted ULS point clouds using TLS source point clouds but not using ALS source point clouds because this could lead to missing points if, e.g., the stem was not completely captured in the ALS point cloud. When using TLS point clouds as source point clouds, we used search radii of 0.3, 0.5 and 1.0 m in the nearest-neighbor search. We then visually examined the extracted ALS and ULS point clouds and chose the search radius achieving the best trade-off between errors of omission and errors of commission. For the extraction using ULS template point clouds, we always used a search radius of 1.0 m.

2.3.4 Tree positions

We define the tree position as the intersection of the tree stem center line with the terrain. To derive the tree positions, we first computed digital terrain models (DTMs) from the ALS point clouds. We then cut a slice through the bottom of the tree point cloud, preferably the TLS or ULS point clouds, if available. We determined the x - y position of the stem as the

mean of the x and y coordinates of all points in the slice. At this position, we queried the elevation of the DTM to retrieve the matching z value. For quality control, the derived positions were visually investigated. In some cases, they had to be corrected either because of DTM errors or because the point cloud did not have enough stem points. If not enough stem points were present to determine the tree stem center at ground level, the x - y positions of the lowest visible stem point were used.

2.4 Tree measurements

Tree measurements were recorded in the field and/or derived from the point clouds. Table 3 gives an overview of the metrics and the data source they were derived from.

2.4.1 Field measurements

Field measurements were conducted in six plots of 1 ha (Fig. 2): BR01, BR03 and BR05 in Bretten and KA09, KA10 and KA11 in Karlsruhe. For each tree, the diameter at breast height (DBH) was measured with a measuring tape at 1.3 m above ground. To determine the crown diameter (CD), the diameter of the estimated dripline (i.e., the line right under the outer circumference of the crown) was measured in two orthogonal directions using a Haglöf Vertex-IV hypsometer. Mean CD was then calculated as the mean of these two distance measures. We define crown base height (CBH) as the height of the lowest branch with a minimum length of 1 m and crown base height green (CBH green) as the height of the lowest green (living) branch with a minimum length of 1 m. We selected the branches fulfilling these conditions by visual

Table 3. Tree measurements and the source(s) they were recorded or computed from. Tree height was only measured from TLS point clouds for understory trees, for which tree height measurements from ALS or ULS would not be reliable. Tree height was only recorded in FM for smaller trees, where the top of the crown was visible from the ground (Sect. 2.4.1). ALS is airborne laser scanning, ULS is UAV-borne laser scanning, TLS is terrestrial laser scanning and FM is field measurements. All height measurements refer to height above the ground level at the stem position. For each tree, there can be multiple values for one tree metric if they were derived from different sources.

Metric	Unit	Description	Source(s)			
1 Tree height	m	Height of the tree	ALS	ULS leaf-on	(TLS)	(FM)
2 Diameter at breast height (DBH)	cm	Stem diameter, measured at 1.3 m above ground	–	–	TLS	FM
3 Crown base height (CBH)	m	Height of the lowest branch	ALS	ULS	–	FM
4 Crown base height (CBH) green	m	Height of the lowest green (living) branch	–	–	–	FM
5 Mean crown diameter (CD)	m	Mean of two orthogonal crown diameters	ALS	ULS	–	FM
6 Crown projection area (CPA)	m ²	Area of the tree crown	ALS	ULS	–	–

estimation and then measured their heights above ground using the hypsometer. Since measuring tree height with the hypsometer is difficult in dense forest stands where high tree tops are barely visible, tree height was only measured for about 10 % of the trees. These were mostly understory trees, where the crown was in direct view. As additional attributes, tree species and state (alive or dead) were recorded. For trees outside of the six field measurement plots, only species and state were determined. Field measurements and single-tree point clouds were matched based on extracted tree positions, the distinct crown shape and branch architecture, and the local neighborhood of the trees. For this, additional field surveys were conducted, in which 3D views of the laser scanning point clouds were used to identify the corresponding trees in the field.

2.4.2 Tree metrics derived from point clouds

In addition to field measurements, tree metrics were estimated from the laser scanning point clouds. For the computation of the metrics, the height values of each tree point cloud were height-normalized by subtracting the z coordinate of the tree position (representing the terrain height at the location of the stem) from all z coordinates in the point cloud.

DBH was estimated only from TLS tree point clouds. Due to the terrestrial view point and close range, many returns are recorded from the stems, allowing for accurate DBH estimation. A slice of the tree point cloud was extracted at a height between 1.28 and 1.32 m above ground. In case the stem was partly occluded, a thicker slice was extracted or the vertical position of the slice was adapted to achieve better results. We projected the slice onto the $x-y$ plane and fit a circle to the points using the random sample consensus (RANSAC) algorithm to derive the diameter using 1000 random samples. For leaning trees, errors may arise from the projection of points to the $x-y$ plane instead of a plane perpendicular to the stem. However, since most of our TLS trees were upright, this error is negligible. Some tree stems have an ellip-

tical rather than a circular stem shape. In these cases (44 of 264 TLS point clouds), an ellipse was fitted to the projected points of the stem slice using least squares (as implemented by Nicky van Foreest: https://github.com/ndvanforeest/fit_ellipse, last access: 12 July 2020). The DBH was then determined as the arithmetic mean of the major and the minor axes of the ellipse. For all trees, the quality of the fit was controlled visually. All figures of the circle/ellipse fitting are included in the Supplement together with a list of trees for which (a) a different slice height was used, (b) the visual assessment suggests low accuracy and (c) TLS-derived DBH values deviate more than 10 % from the values measured in the field.

Tree height was derived as the z coordinate of the highest tree point, normalized by the elevation of the tree position, i.e., the base of the tree.

CBH was determined by dividing the point cloud into height sections of 0.1 m and calculating the maximum $x-y$ distance between any two points in the section. Starting from the bottom, we iterate over the height sections. Once the maximum horizontal point distance exceeded a threshold of DBH + 1 m (if no DBH measurement was available, a default of 0.5 m was used), the center of the height section is defined as the CBH (Fig. 6) and the iteration is terminated. Because of the fixed section height, CBH estimates have decimeter resolution.

The tree crown is defined by all points above the CBH. Crown projection area (CPA) was calculated in two different ways:

- as the area of the 2D ($x-y$) *convex hull* of all crown points using the Quickhull algorithm (Barber et al., 1996)
- as the area of the 2D ($x-y$) *concave hull* of all crown points using the k -nearest-neighbor approach by Moreira and Yasmina Santos (2007) as implemented by Craig (2017).

Lastly, mean CD was computed as the mean of the largest diameter and the largest perpendicular diameter of the concave hull (Fig. 6).

3 Results

The data records are split into two parts:

- the full TLS and ULS point clouds and extracted ALS subsets covering the ULS, TLS and field measurement plots (see Fig. 2)
- the extracted single-tree point clouds and respective measured and point-cloud-derived tree metrics.

The folder structure is visualized in Fig. 7.

3.1 LAS point format

All point clouds are stored in ASPRS LAS 1.4 (ASPRS, 2013) or ASPRS LAS 1.2 format (ASPRS, 2008), compressed (lossless) to LAZ. The field “Point source ID” holds the IDs of the flight lines or scan positions that the points originated from. All LAZ files contain the extra bytes amplitude [dB], reflectance [dB] and (pulse shape) deviation [] as exported by RIEGL systems. The amplitude is calibrated as the ratio of the optical power of the reflected light to the detection threshold of the instrument and depends on the distance of the target to the scanner (Pfennigbauer and Ullrich, 2010). The reflectance, however, is distance-independent and determined by the properties of the target that was hit by the ray. Reflectance is given as the ratio of the amplitude of the hit target to the amplitude of the target the instrument was calibrated with, i.e., a diffuse white target (Pfennigbauer and Ullrich, 2010). The pulse shape deviation indicates the degree to which the shape of the received pulse deviates from a device-specific reference pulse shape.

3.2 Full forest plot or acquisition records

In order to also capture the neighborhood context of the single tree, understory and terrain information, we provide the larger-area georeferenced point clouds of each platform. These include 31 TLS point clouds stored in LAZ files. For each acquisition, we provide a tab-separated .txt file containing the coordinates of the scan positions. A total of 20 LAZ files are available containing the ULS point clouds acquired under leaf-on and leaf-off conditions as summarized in Table 2. Note that the ULS leaf-on data for plots BR03 and BR08 are included in one single LAZ file, and no ULS data are available for plot BR04. For each acquisition, the trajectory is provided as a tab-separated .txt file, containing continuous records of the location and orientation of the sensor in the air. The “Time [s]” in the trajectory files corresponds with the “GPSTime” in the respective LAZ point cloud files and represents seconds since beginning of the

respective GPS week (ASPRS, 2013). Finally, we provide 12 LAZ files with extracted ALS point clouds, one for each plot (Fig. 2). ALS point clouds of plots BR01, BR03, BR05, KA09, KA10 and KA11 are 300 m × 300 m in size and encompass the 100 m × 100 m plots in which field measurements were recorded. ALS point clouds of plots BR02 and BR06 are 200 m × 200 m and ALS point clouds of BR04, BR07, BR08 and SP02 are 140 m × 140 m in size. For these six plots (BR02, BR04, BR06, BR07, BR08 and SP02), no field measurements are available. We provide the trajectory points for the respective parts of the flight strips covering the area in tab-separated .txt files. All ALS point clouds spatially overlap with the TLS and ULS acquisitions conducted in the respective plots.

All point clouds and the coordinates of the scan positions and trajectories are in the same coordinate reference system: ETRS89/UTM zone 32N; EPSG:25832; ellipsoidal height, GRS80.

3.3 Single tree point clouds and metrics

Point clouds and point-cloud-derived metrics are provided for 1491 individual trees of in total 22 different species. An overview of tree species and the respective number of trees is given in Table 4. Field-measured metrics are available for 1060 of the trees. Tree point clouds acquired from all three platforms, i.e., ALS, TLS and ULS (leaf-on), are provided for 249 trees. A total of 1168 tree point clouds were extracted both from ULS leaf-on and ULS leaf-off data. A summary of all available data types per tree is given in Table 5 and Fig. 8. Figure 4 shows the different characteristics of the point clouds acquired from the different platforms and in the different canopy conditions. When comparing the TLS leaf-on point clouds with the ULS leaf-off point clouds, it is clearly visible that the branches hang down more in the summer when they are full of leaves than in the fall or winter when they are free of foliage.

There are multiple reasons for the different available data types per tree:

- TLS acquisitions did not cover the entire ALS/ULS acquisitions but only selected locations, so only 246 TLS point clouds of trees are available.
- No ULS acquisition was performed in plot BR04.
- ALS point clouds of understory trees with very few points were discarded. This concerned only silver firs in plot SP02 (AbiAlb_SP02_01 to AbiAlb_SP02_05), which had between 11 and 247 ALS points.
- Some trees were only extracted manually from ALS point clouds, and these were not used for automatic extraction due to the lower resolution compared to ULS and TLS point clouds, which would cause information loss (e.g., missing parts of the stem).

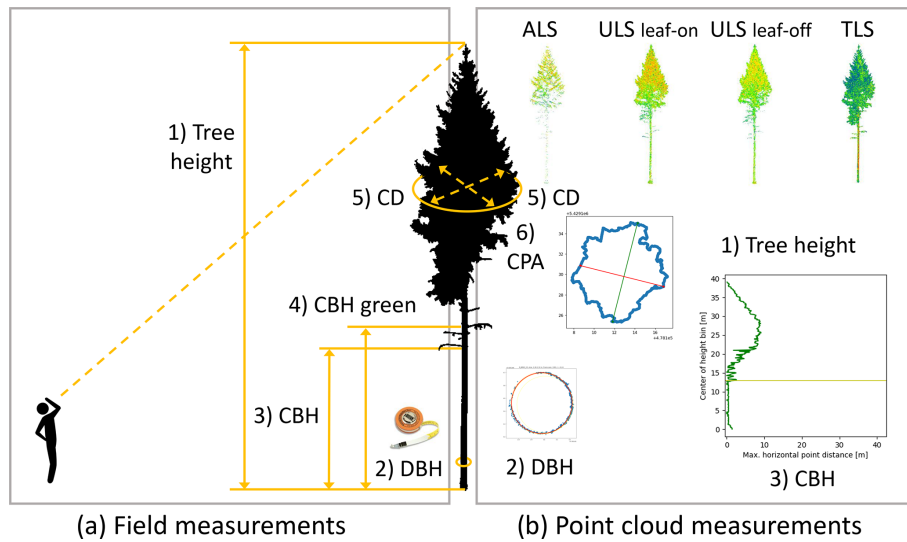


Figure 6. Overview of single tree measurements (**a**) recorded in the field and (**b**) derived from the point clouds. Numbers correspond to Table 3. Icon on the left (“man looking up”) by DonBLC, <https://thenounproject.com/> (last access: 3 August 2021). Picture of diameter tape from <https://www.forestry-suppliers.com/> (last access: 3 August 2021).

Table 4. Number of trees of each species in the dataset.

Species	SpeciesID	No. of trees
<i>Abies alba</i> Mill.	AbiAlb	25
<i>Acer campestre</i> L.	AceCam	7
<i>Acer pseudoplatanus</i> L.	AcePse	39
<i>Betula pendula</i> Roth	BetPen	6
<i>Carpinus betulus</i> L.	CarBet	94
<i>Fagus sylvatica</i> L.	FagSyl	398
<i>Fraxinus excelsior</i> L.	FraExc	11
<i>Juglans regia</i> L.	JugReg	19
<i>Larix decidua</i> Mill.	LarDec	30
<i>Picea abies</i> (L.) H. Karst.	PicAbi	205
<i>Pinus sylvestris</i> L.	PinSyl	158
<i>Prunus avium</i> (L.) L.	PruAvi	19
<i>Prunus serotina</i> Ehrh., nom. cons.	PruSer	7
<i>Pseudotsuga menziesii</i> (Mirb.) Franco	PseMen	191
<i>Quercus petraea</i> (Matt.) Liebl.	QuePet	156
<i>Quercus robur</i> L.	QueRob	7
<i>Quercus rubra</i> L.	QueRub	111
<i>Robinia pseudoacacia</i> L.	RobPse	1
<i>Salix caprea</i> L.	SalCap	1
<i>Sorbus torminalis</i> (L.) Crantz	SorTor	1
<i>Tilia spec.</i> L.	TilSpec	4
<i>Tsuga heterophylla</i> (Raf.) Sarg.	TsuHet	1
		1491

Tree properties are provided in two tab-separated .txt files:

- General tree characteristics such as the species and the tree position in geographic coordinates and in UTM coordinates are listed in a tab-separated .txt file with suffix “_general”.

- Tree metrics are provided in a tab-separated .txt file with suffix “_metrics”. There is one row for each measurement source (e.g., field inventory measurement (FI) and ALS) and one column for each tree metric.

We furthermore provide all tree metadata in GeoJSON files, including geometry (position), properties (field measurements and point cloud metrics) and data (point cloud data filenames and metadata). These files can be loaded into common GIS software to visualize the tree positions and access the data.

4 Quality assessment

In the following, we describe how we assessed different aspects of data quality for our dataset. Table 6 summarizes all quality indicators related to point cloud alignment and georeferencing.

4.1 Airborne and UAV-borne laser scanning (ALS and ULS)

4.1.1 Positional accuracy

Positional accuracy of the ULS data was determined using roof-shaped wooden targets of 1 m length and 0.6 m width (for one side of the roof). The two planes of the roofs were recorded with four points each using a Leica Viva GS10/GS15 RTK GNSS unit tied into the SAPOS correction network (<https://www.sapos-bw.de>, last access: 24 June 2022). A visual inspection of the wooden target point clouds and the GNSS reference measurements showed good alignment, with differences in the range, that was expected due to the limited scanner and RTK accuracies (Fig. 9).

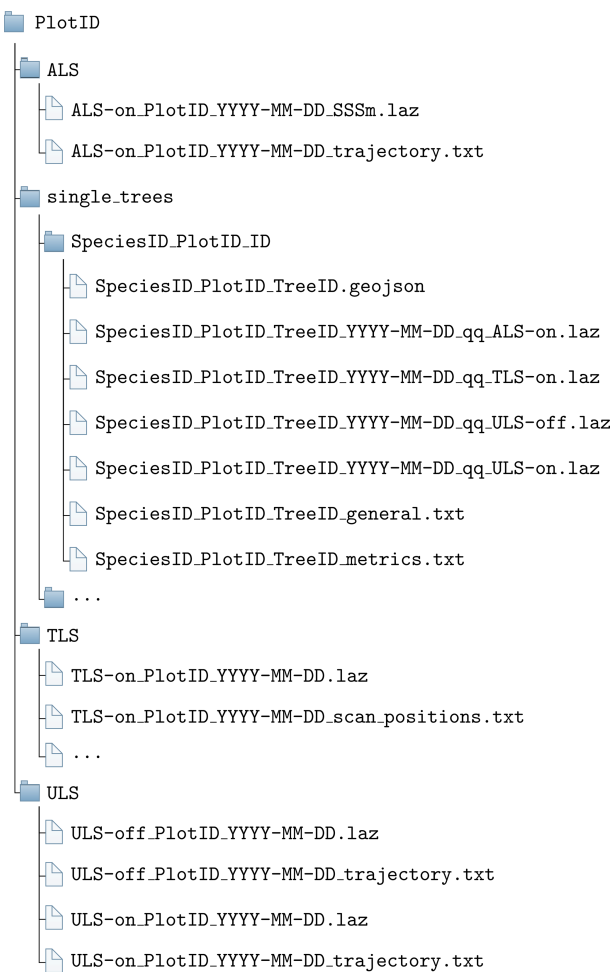


Figure 7. Folder structure for a single forest plot. PlotID is the ID of the forest plot, e.g., BR01; SpeciesID is the ID of the tree species, e.g., AcePse; see Table 4; TreeID is the unique (in combination with PlotID and SpeciesID) identifier for the tree; YYYY-MM-DD is the day of acquisition; qq is the quality indicator, e.g., q2; on/off is the canopy condition; and SSSm is the side length of the ALS forest plot in meters, e.g., 300 m. The ALS folder contains only one point cloud per plot. Multiple point clouds may be within the ULS folder due to different acquisition times and in the TLS folder due to different acquisition times and locations (in case of several acquisitions in the same plot on the same day, a suffix is added to distinguish the acquisitions, i.e., “_A”, “_B”, etc.). The single_trees folder always contains several subfolders, one for each tree.

Absolute altitude accuracy of ALS data was determined by MILAN Geoservices GmbH using reference tiles recorded with ULS by the 3DGeo Research Group of Heidelberg University. The height of selected reference points was compared to the median of ALS points within a radius of 0.2 m (Bretten) and 0.3 m (Karlsruhe). The mean altitude differences (standard deviations) were -0.003 m ($\pm 0.023 \text{ m}$), 0.006 m ($\pm 0.016 \text{ m}$), -0.016 m ($\pm 0.026 \text{ m}$), -0.028 m and ($\pm 0.029 \text{ m}$) for the four tiles in Bretten and -0.016 m ($\pm 0.017 \text{ m}$) for the tile in Karlsruhe. The quality of these ref-

erence tiles was, in turn, ensured by the same method as for the ULS data in general; see above.

Positional (horizontal) accuracy of the ALS data was controlled by MILAN Geoservice GmbH using building edges (i.e., stable surfaces). A building layout derived from TLS data, which was acquired by the 3DGeo Research Group and georeferenced with RTK GNSS, was overlaid with the building layout derived by digitizing the classified ALS point cloud to investigate the positional accuracy.

A further independent assessment of positional and altitude accuracy was conducted by the 3DGeo Research Group Heidelberg by comparing points sampled by ULS and ALS on roofs and other stable surfaces in control areas. Figures of the visual assessment are included in Appendix B in the metadata document published along with the dataset on the data repository PANGAEA (https://download.pangaea.de/reference/109167/attachments/SYSSIFOSS_2019-2020_meta_4.pdf, Weiser et al., 2022b). To obtain quantitative measures, we computed cloud-to-cloud distances between these ALS and ULS point clouds of the stable areas (six in Karlsruhe and three in Bretten). Resulting mean distances were between 0.03 and 0.06 m, with standard deviations between 0.01 and 0.023 m. This confirmed the high accuracy of the alignment of the datasets.

4.1.2 Strip alignment

The internal alignment of ALS and ULS flight strips was investigated by the 3DGeo Research Group by quantifying the height differences between the flight strips with OPALS (version 2.3.2). For ALS, strip differences were quantified for the extracted plot point clouds (with the extents as shown in Fig. 2). The ULS point clouds were cropped to the 1 ha plots for the assessment of the strip alignment to exclude points at the flight line edges.

For both datasets, single strip point clouds were first filtered for last returns. Second, grids of the standard deviation of the interpolated height (σ_Z) and of the distances between grid points and the center of gravity of data points (eccentricity) were computed to derive a mask of areas suited for the quality check. For the quantification of strip differences, areas with $\sigma_Z \geq 0.1 \text{ m}$ and eccentricity $\geq 0.08 \text{ m}$ were masked. This concerns most areas with high vegetation, where strip differences cannot be quantified reliably.

For the ALS point clouds, median absolute strip differences were below 5 mm for 10 of 12 plots. The maximum median value was 11 mm. $\sigma(\text{MAD})$ was between 17 and 51 mm¹. For ULS leaf-on point clouds, median absolute differences were up to 14 mm (mean: up to 55 mm). For ULS

¹ $\sigma(\text{MAD})$ is the median absolute deviation to median (MAD) scaled by 1.4826 to obtain a robust estimator for the standard deviation σ under the assumption of a normal distribution; <https://opals.geo.tuwien.ac.at/html/stable/ModuleHisto.html> (last access: 24 June 2022).

Table 5. Number of trees per plot and data source. Note that most trees were measured from different platforms and at different times. ULS leaf-off data are available for 1173 trees. Of these, 133 trees were measured in autumn 2019, 537 trees were measured in spring 2020 and 503 trees were measured both in autumn 2019 and spring 2020.

Plot	Data source						
	ALS	ULS	ULS (leaf-off)		TLS	Field	Any
			(leaf-on)	Autumn 2019			
BR01	514	503		503	15	410	514
BR02	42	42		–	41	42	42
BR03	195	141		–	141	41	162
BR04	9	–		–	–	9	9
BR05	278	278		–	278	35	224
BR06	29	29		–	29	29	29
BR07	15	16		–	15	16	–
BR08	13	13		–	12	13	–
SP02	17	17		–	21	22	–
KA09	177	136	133	–	15	98	177
KA10	40	14	–	–	11	35	40
KA11	151	97	–	–	16	131	151
				636	1040		
All	1480	1286		1173	264	1060	1491

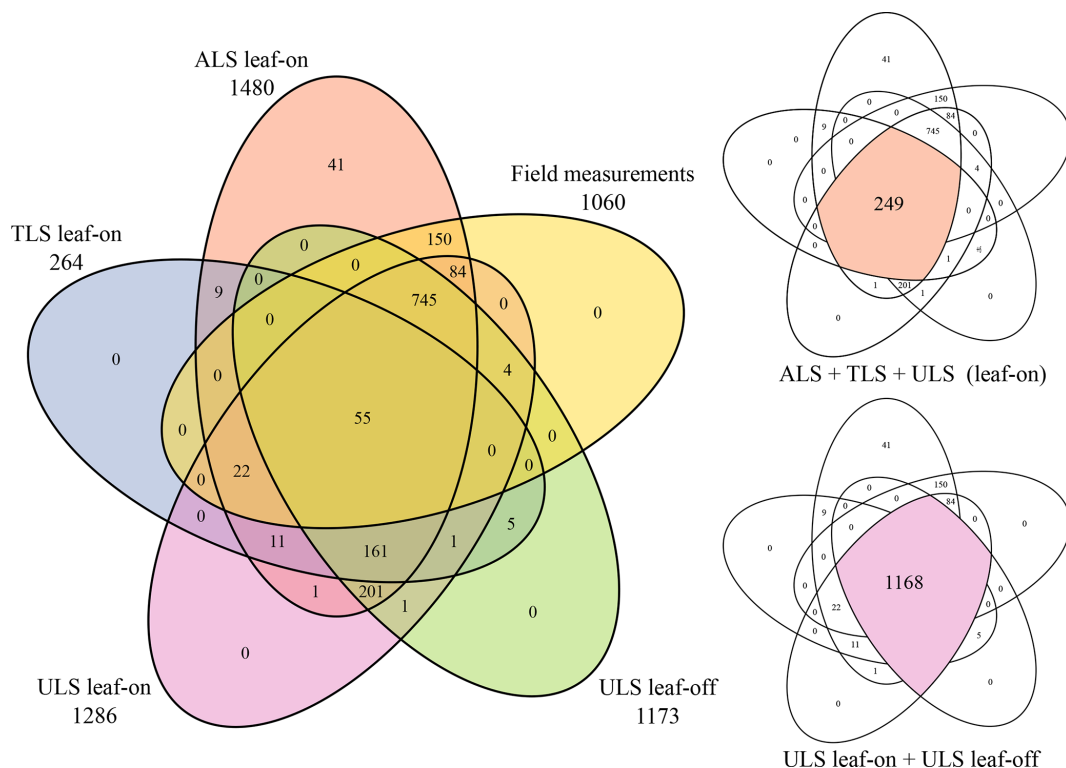


Figure 8. Venn diagrams showing the number of trees covered by the different acquisitions.

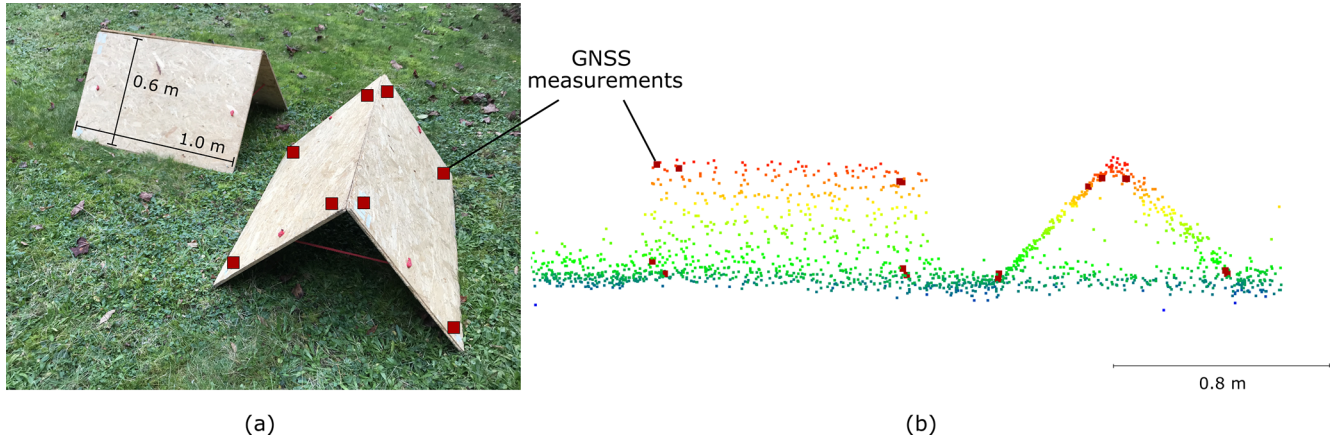


Figure 9. Roof-shaped wooden targets used for assessing the positional accuracy of the ULS point cloud. **(a)** Setup in the field. The two planes of each roof are 1 m by 0.6 m in size. The red squares in both images mark the points where GNSS measurements are taken. **(b)** View in a point cloud viewer. The ULS point cloud is colored by z coordinate, and the GNSS measurements are shown as large red squares. The georeferencing quality is considered good if the ULS points on the roofs agree closely with the GNSS reference measurements, as shown in this example.

leaf-off point clouds, median absolute strip differences were only up to 2 mm (mean: below 20 mm for 10 acquisitions, 51 and 62 mm for the remaining two acquisitions), suggesting that the large values in the leaf-on differences are a remaining influence from vegetation. Histograms and maps of strip differences for ALS and ULS data are included in Appendix A in the metadata document published along with the dataset on the data repository PANGAEA (Weiser et al., 2022b).

4.2 Terrestrial laser scanning (TLS)

4.2.1 Positional accuracy and alignment to ULS point clouds

TLS point clouds were georeferenced by coarsely registering them to the ULS data via tree stem matching, followed by a fine alignment with the ICP algorithm. Before running the ICP, we created downsampled TLS point clouds with the octree filter in RiSCAN PRO with voxel sizes of 0.05 m. For each voxel of the octree, a new point is created by taking the center of gravity for all the points within each voxel. We performed an ICP adjustment with five iterations, keeping the ULS point cloud fixed while transforming the TLS point cloud. With these settings, we achieved mean point-to-plane distances of less than 2 mm, with standard deviations between 120 and 140 mm.

For 13 of the 31 point clouds, we still observed significant shifts in a visual assessment and repeated the ICP with revised settings: we used the ULS point cloud as moving, preferably the one acquired under leaf-off canopy condition (if available) due to the better representation of the stems, and the TLS point clouds as fixed point clouds. This means that the subset of points for which correspondences are established and to which planes are fitted to subsequently mini-

mize point-to-plane distances are selected from the TLS point cloud. This is likely to achieve better results because the TLS point cloud has higher point density (allowing for better plane fit) and higher accuracy. We used the full-resolution TLS point clouds and in some cases filtered for points below 15 or 10 m to exclude crown points. For the tree crowns, the coverage of TLS and ULS point clouds is very different, and there are many moving objects (branches and leaves). We increased the number of iterations to up to 10. We then applied the inverse output transformation matrix to the TLS point cloud to ensure that the final georeferencing is derived from the ULS data. This resulted in mean point-to-plane distances of below 4 mm, with standard deviations of 50–100 mm. More importantly, the visual alignment improved considerably.

Because of the lack of bigger planar areas in the scene, the influence of moving branches and leaves, the different viewing geometries and resulting occlusions of the ULS and TLS point clouds, and the sensor accuracy limits, it is expected that no sub-millimeter point-to-plane distances were achieved, and the standard deviation is comparably high. The final alignment is sufficient for our main intention, i.e., the extraction of trees from ULS and ALS point clouds using template TLS point clouds. A visual impression of the quality of the alignment between the datasets acquired from the different platforms is given in Fig. 4. The visual assessment and the low mean distances suggest no remaining systematic shifts.

4.2.2 Internal co-registration of single scan positions

Co-registration quality of scan positions relative to the main stable position for each plot was assessed in two stages. In the first stage we investigated differences computed in the least-

squares algorithm of the Multi Station Adjustment performed in RiSCAN PRO. The overall average of the standard deviation of registration error (RMSE) was 5 mm, with a maximum of 8 mm. In the second stage, a visual assessment was conducted by projecting a narrow section of the point cloud onto a plane and coloring the points by their scan position. We used stem slices for assessing horizontal registration errors and cylindrical reflective targets for assessing vertical registration errors. Horizontal stem slices were manually extracted for selected trees with an approximate section width of 0.2 m. To minimize the influence of wind effects, stem slices were cut out from low heights above ground where tree stems are very stable. This was especially relevant for younger trees, where tree stems are smaller in diameter and therefore more prone to movement. No significant vertical registration errors were present in any of the plots. In most of the acquisitions (26 of 31), no or very small (< 10 mm) horizontal registration errors were observed. In five acquisitions, the maximum horizontal registration error was estimated to be between 10 and 20 mm. Appendix C in the metadata document published along with the data (Weiser et al., 2022b) shows the assessment of horizontal and vertical TLS registration errors.

4.3 Quality of single-tree point clouds

Tree point clouds were assigned a quality tag from highest (q1) to lowest (q6). Reasons for lower grades include

- segmentation errors, e.g., additional branches in the point cloud;
- extraction errors, e.g., additional points from neighboring trees in the point cloud because of the fixed search radius used for the automatic kNN-based extraction;
- missing parts/occlusion of tree parts;
- wind effects (in case of TLS);
- scan position or flight strip alignment errors.

The quality tags were subjectively assigned by different operators. For most trees that were extracted automatically using the kNN algorithm, the quality was set to one lower than the source point cloud. The quality tag therefore provides a rough idea of the point cloud quality but is not guaranteed to be comparable across the entire dataset.

4.4 Quality of the tree metrics

The quality of the tree metrics computed from the tree point clouds depends on the accuracy of the tree point cloud segmentation and the point density of the tree point cloud. Error of commission in the segmentation may cause higher tree height, mean CD and CPA values, and lower CBH values, while error of omission or a low point density may cause the

opposite. In particular, ALS tree point clouds of understory trees have a low point density, and thus the computed metrics might differ from the field-measured metrics. As field measurements were conducted from the ground, field-measured height, mean CD and CBH of high trees have higher uncertainty than those of smaller trees. It is difficult to consider either the field measurements or the point-cloud-derived metrics as true reference. By comparing field-measured and point-cloud-derived metrics, we can nevertheless get an idea of the error ranges and potential biases.

Tree metrics derived from different sources are highly correlated (except CBH). The Pearson correlation coefficient (ρ) of DBH measured in the field and DBH computed from the TLS tree point clouds is 0.98, and the root-mean-square error (RMSE) is only 3.5 cm. The correlation of tree heights derived from different laser scanning point clouds is 1.00, and the RMSE is 0.3–0.4 m. This is lower than the search radius of 0.5 m, which was mostly used for the automatic tree extraction. The deviation of field-measured tree height to point cloud tree height is higher (RMSE = 2.5–2.7 m, $\rho = 0.96$). Field-measured tree heights might be less accurate, especially in cases of high trees with flat crowns, where the tree top was not visible from the ground. The RMSE of mean CD is 0.7–1.2 m between different point cloud metrics ($\rho = 0.97$ –0.98) and 1.5–1.6 m ($\rho = 0.88$ –0.90) between field measurements and point cloud metrics. Absolute crown diameters are between 2 and 22.1 m, with a median value of 7.7 m (values based on field measurements). Higher deviations in CD between field measurements and point cloud metrics occur for trees with an elongated horizontal crown extent, where the direction of the two orthogonal diameter measurements is more important than for crowns with nearly circular circumference. The CD values computed from point clouds might be overestimated for leaning trees because the part of the stem which is not covered by the crown may still be included in the crown extent if it is above the estimated CBH. Field-measured diameters might be of lower accuracy for high tree crowns where the outer crown circumference was difficult to estimate. The definition and determination of CBH are difficult, both in the field and in the point cloud, resulting in high deviation of CBH values derived from different data sources. The RMSE of CBH computed from different laser scanning point clouds is 4.8–6.9 m ($\rho = 0.66$ –0.76). On the one hand, the point-cloud-derived CBH is sensitive to segmentation errors, especially in the case of the automatic tree extraction from template point clouds. If understory points are wrongly assigned to a tree point cloud, the CBH may be underestimated. On the other hand, the lowest branches may not be sampled well in ULS and especially ALS point clouds; hence the CBH may be overestimated. The field-measured CBH accuracy is negatively affected by an over- or underestimation of branch lengths resulting in a wrong selection of the lowest branch defining the CBH. The RMSE between field-measured and point-cloud-derived CBH is 4.0–5.1 m, and ρ is 0.59–0.72 m. Figure 10

Table 6. Summary of the different indicators for georeferencing and alignment quality. SD is the standard deviation.

Quality aspect	Quality indicator	Quantitative results	Qualitative results
ULS georeferencing accuracy	Agreement of GNSS measurements on roof-shaped targets with ULS points (Sect. 4.1.1)		Visual assessment showed no evident systematic errors
ALS georeferencing accuracy	Height difference between ALS and ULS point clouds in stable areas (Sect. 4.1.1)	Mean (per area) = -0.028 to 0.006 m SD (per area) = 0.016 to 0.029 m	Visual assessment (Weiser et al., 2022b, Appendix B)
	Cloud-to-cloud distances between ALS and ULS point clouds in (different) stable areas (Sect. 4.1.1)	Mean (per area) = 0.03 to 0.06 m SD (per area) = 0.01 to 0.023 m	
	Agreement of a TLS-derived building layout with the ALS point cloud		Visual assessment showed no evident systematic errors
ULS strip alignment	Flight strip differences per acquisition (Sect. 4.1.2)	Leaf-on: Median ≤ 0.014 m Leaf-off: Median ≤ 0.002 m	Histograms and maps in Weiser et al. (2022b), Appendix A
ALS strip alignment	Flight strip differences per plot (Sect. 4.1.2)	Median ≤ 0.005 m for 10 of 12 plots, Largest median value = 0.011 m	Histograms and maps in Weiser et al. (2022b), Appendix A
TLS scan position alignment	RMSE of the registration error (as quantified in RiSCAN PRO)	Mean (over all acquisitions): 0.005 m Largest mean value = 0.008 m	
TLS scan position alignment	Differences between point clouds from different scan positions, quantified on stem slices (Sect. 4.2.2)	≤ 0.02 m	Visual assessment (Weiser et al., 2022b, Appendix C)
TLS georeferencing	Point-to-plane distances between the TLS and ULS point clouds after the ICP adjustment (Sect. 4.2.1)	Mean ≤ 0.004 m SD = 0.05 to 0.014 m	Visual assessment showed no evident systematic errors

shows scatter plots of field-measured compared to point-cloud-derived DBH, tree height, mean CD and CBH.

5 Usage notes

There are different methods to clean point clouds prior to further processing, e.g., applying the statistical outlier removal (SOR, Rusu et al., 2008) as implemented, e.g., in the Point Cloud Library (PCL; Rusu and Cousins, 2011) or in Cloud-Compare. When working with the TLS data, we recommend filtering the point cloud by pulse shape deviation (as defined by *RIEGL*). This deviation can give an idea of the reliability of the range measurement, so excluding points with high deviation can improve the overall quality of the point cloud (Pfennigbauer and Ullrich, 2010). We found a value of 50 to be a suitable threshold.

Because we define the tree position as the position of the stem at ground level, this position (in ETRS89/UTM 32N coordinates; EPSG:25832, ellipsoidal height, GRS80) can be used to normalize the height values of the point clouds to derive heights above ground.

Point clouds can be visualized and processed using the open-source software CloudCompare, other lidar software like OPALS (Pfeifer et al., 2014) or LAStools (Rapidlasso GmbH, 2020), or custom code.

We created the Python software package `pytree3db` (Höfle et al., 2022), which provides a simple database interface and REST API to perform queries on a database of tree objects. `pytree3db` allows trees to be selected using different filters, maps of the selection results to be viewed and data to be exported in different formats (LAZ point clouds, GeoJSON files, CSV files).

Software for the generation of tree models from TLS tree point clouds includes TreeQSM (Raumonen, 2020; Raumonen et al., 2013), SimpleForest (Hackenberg et al., 2015; Hackenberg, 2021), PlantScan3D (Boudon, 2021) and AdTree (Du et al., 2019; Nan et al., 2021). These tools reconstruct the woody structure of the trees and therefore require input point clouds without leaf points. Leaves may be removed from TLS point clouds using spectral and geometric features, as proposed in multiple studies (Krishna Moorthy et al., 2020; Vicari et al., 2019; Wang et al., 2020; Yun et al., 2016; Zhou et al., 2019) and implemented in different software packages (TLSeparation, Vicari, 2021; LeWoS, Wang, 2020). Structural tree reconstruction algorithms may also perform well on some of the ULS leaf-off point clouds, for which no leaf removal is required. Trees may furthermore be reconstructed using voxel-based approaches (Weiser et al., 2021).

To perform simulation studies with the reconstructed 3D forest scenes, e.g., to conduct sensitivity analyses, radiative

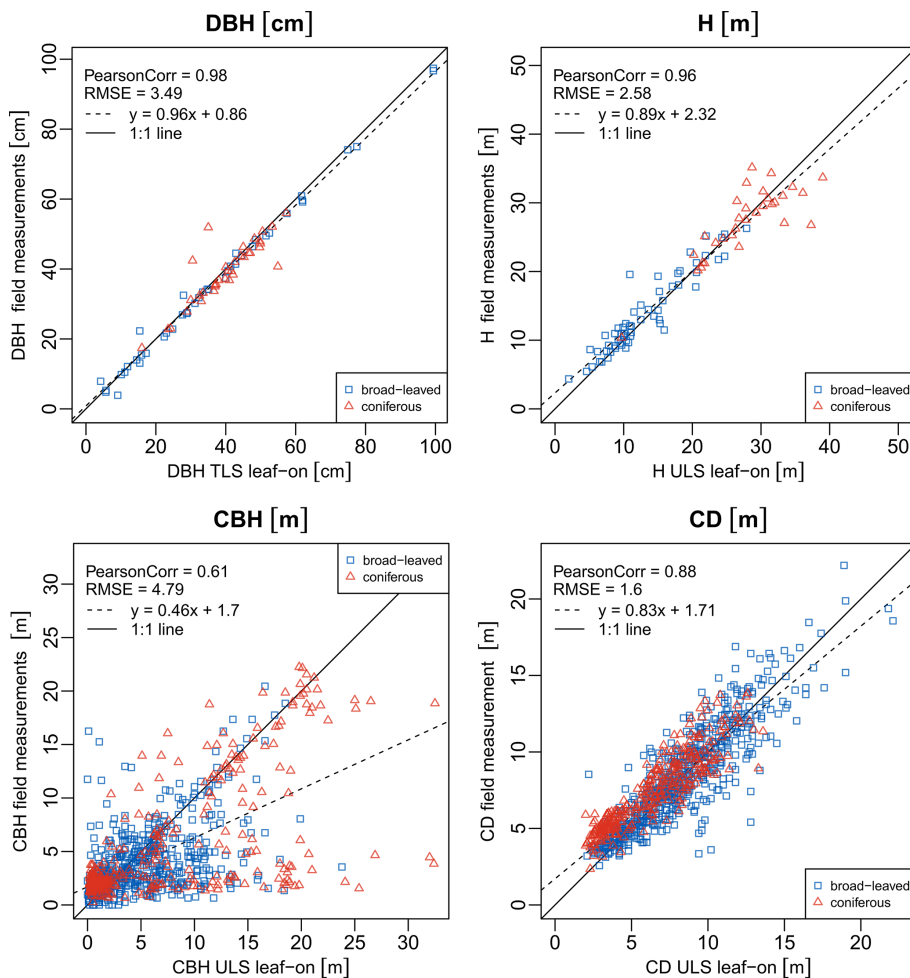


Figure 10. Scatter plots of metrics computed from tree point clouds and measured in the field. Pearson correlation, root-mean-square error and the equation of a linear model fit to the data are given. DBH is the diameter at breast height, H is the tree height, CBH is the crown base height and CD is the crown diameter.

transfer models such as DART (Gastellu-Etchegorry et al., 2004), librat (Calders et al., 2013; Lewis and Muller, 1992; Lewis, 1999) or Rayspread (Widlowski et al., 2006) may be used. DART also allows lidar to be simulated. Furthermore, there are specialized lidar simulators such as HELIOS++ (Winiwarter et al., 2022, 2021). The point clouds presented here can be used as scene parts for HELIOS++ after converting LAZ files to ASCII files, e.g., using LAStools:

```
las2txt -i <pointcloud.laz>
        -o <pointcloud.xyz>
        -oparse xyz
```

and using the xyzloader of HELIOS++ (<https://github.com/3dgeo-heidelberg/helios/wiki/Scene#xyz-point-cloud-loader>, last access: 24 June 2022). Alternatively, the trees can be loaded as DetailedVoxels (<https://github.com/3dgeo-heidelberg/helios/wiki/Scene#detailedvoxels>, last access: 24 June 2022), e.g., after deriving voxel-based plant area density estimates using the software

AMAPVox (Vincent et al., 2017; Weiser et al., 2021, <https://amap-dev.cirad.fr/projects/amapvox>, last access: 24 June 2022).

Our dataset can furthermore be used as a benchmark and testing dataset for tree segmentation and species classification algorithm. This was shown by Fu et al. (2022), who used the TLS point clouds of this dataset for testing the accuracy of their individual tree segmentation algorithm. It may be used to explore the differences between the point cloud measurements from different acquisition platforms and the tree and forestry metrics that can be derived from them. Our dataset can be valuable for developing and testing algorithms on the retrieval of forestry parameters on the single tree or the plot level. Furthermore, open forest datasets like this can serve as reference datasets for the calibration and validation of spaceborne data products like biomass maps from satellite images or from spaceborne lidar data such as the NASA's Global Ecosystem Dynamics Investigation (GEDI; Dubayah et al., 2020).

6 Code and data availability

Our dataset is published with PANGAEA and available at <https://doi.org/10.1594/PANGAEA.942856> (Weiser et al., 2022a). For each forest plot, one zip folder is provided, containing the forest plot point clouds with trajectory or scan position information and the single-tree point clouds and measurements. Point clouds of the full-coverage airborne laser scanning acquisitions (covering around 65 km² in Karlsruhe and 32 km² in Bretten) and associated full-waveform data are not part of the PANGAEA dataset but are available from the authors on reasonable request.

Python code used for processing the dataset is openly available on GitHub (<https://doi.org/10.5281/zenodo.6759913>, Weiser, 2022). The code uses the libraries NumPy, pandas, laspy, pykdtree, SciPy, jsonschema and Matplotlib. The scripts for georeferencing use the Python bindings of OPALS (Pfeifer et al., 2014) modules and were tested with versions 2.3.1 and 2.3.2. Please contact the authors for guidance on using the code.

7 Conclusions

Our dataset encompasses terrestrial and airborne laser scanning point clouds acquired from three different platforms: a static tripod, an uncrewed aerial vehicle (UAV) and a fixed-wing aircraft. We thus obtain georeferenced point cloud rep-

resentations of the overlapping forest areas at different resolutions and from different viewpoints. UAV-borne laser scanning (ULS) point clouds were furthermore recorded in different seasons, under leaf-on and leaf-off canopy conditions. From the full-coverage point clouds of the plot acquisitions, which are also provided within this publication, we identified and extracted individual single trees, resulting in 4205 point clouds of 1491 individual trees of 22 different species. Most of these trees were captured by airborne and UAV-borne laser scanning. For 249 trees, high-resolution terrestrial laser scanning point clouds are additionally available. We recorded tree measurements in the field, which we compare to and complement with point-cloud-derived tree metrics. This results in single tree forest inventory data with one to five 3D point cloud representations of each tree. The full aerial point clouds, the single-tree point clouds, and the measured and point-cloud-derived tree metrics have high reuse value for numerous applications. We identified the following main areas for such applications: (i) development of allometric equations between 3D tree structures and forest inventory variables; (ii) application as training data for machine learning applications such as tree instance segmentation, tree species classification or tree metric computation; and (iii) creation of detailed tree models for lidar simulations or for computer rendering.

Appendix A

Table A1. Forest characteristics of full inventory plots of 1 ha. Values are given for all trees in the plot (bold) and for trees of each species separately. For the number of trees and the basal area, both absolute (abs.) and relative (rel.) values are provided. It should be noted that point clouds were not extracted for every tree in these plots.

Plot	Species	No. of trees		Basal area [$\text{m}^2 \text{ha}^{-1}$]		Percentage of dead trees	Median height [m]
		abs.	rel.	abs.	rel.		
BR01	all	738	(100 %)	30.96	(100 %)	11 %	14.0
	<i>Acer campestre</i> L.	5	(1 %)	0.17	(1 %)	0 %	7.9
	<i>Acer pseudoplatanus</i> L.	12	(2 %)	0.05	(0 %)	0 %	9.8
	<i>Carpinus betulus</i> L.	118	(16 %)	1.10	(4 %)	1 %	8.3
	<i>Fagus sylvatica</i> L.	225	(30 %)	15.29	(49 %)	1 %	18.9
	<i>Fraxinus excelsior</i> L.	23	(3 %)	0.18	(1 %)	9 %	12.0
	<i>Larix decidua</i> Mill.	6	(1 %)	0.90	(3 %)	0 %	33.8
	<i>Picea abies</i> (L.) H. Karst.	163	(22 %)	3.86	(12 %)	34 %	15.8
	<i>Pinus sylvestris</i> L.	2	(0 %)	0.43	(1 %)	0 %	29.8
	<i>Prunus avium</i> (L.) L.	26	(4 %)	0.47	(2 %)	0 %	13.8
	<i>Pseudotsuga menziesii</i> (Mirb.) Franco	21	(3 %)	5.66	(18 %)	0 %	36.4
	<i>Quercus petraea</i> (Matt.) Franco	121	(16 %)	2.64	(9 %)	9 %	13.7
	<i>Salix caprea</i> L.	1	(0 %)	0.05	(0 %)	0 %	16.4
	<i>Sambucus nigra</i> L.	14	(2 %)	0.06	(0 %)	57 %	5.8
	unidentified coniferous	1	(0 %)	0.10	(0 %)	100 %	27.4
BR03	all	473	(100 %)	42.00	(100 %)	5 %	20.4
	<i>Abies alba</i> Mill.	28	(6 %)	3.75	(9 %)	4 %	26.5
	<i>Acer campestre</i> L.	4	(1 %)	0.08	(0 %)	0 %	10.4
	<i>Acer pseudoplatanus</i> L.	24	(5 %)	0.70	(2 %)	0 %	9.2
	<i>Betula pendula</i> Roth	1	(0 %)	0.07	(0 %)	100 %	18.2
	<i>Carpinus betulus</i> L.	123	(26 %)	1.82	(4 %)	5 %	11.0
	<i>Corylus avellana</i> L.	3	(1 %)	0.01	(0 %)	33 %	6.1
	<i>Euonymus europaeus</i> L.	2	(0 %)	0.00	(0 %)	0 %	4.1
	<i>Fagus sylvatica</i> L.	50	(11 %)	2.21	(5 %)	0 %	11.8
	<i>Fraxinus excelsior</i> L.	6	(1 %)	0.19	(0 %)	0 %	20.8
	<i>Juglans regia</i> L.	2	(0 %)	0.00	(0 %)	0 %	6.0
	<i>Metasequoia glyptostroboides</i> Hu et Cheng	2	(0 %)	0.16	(0 %)	0 %	23.3
	<i>Picea abies</i> (L.) H. Karst.	10	(2 %)	0.51	(1 %)	20 %	21.2
	<i>Prunus avium</i> (L.) L.	6	(1 %)	0.20	(0 %)	0 %	13.1
	<i>Pseudotsuga menziesii</i> (Mirb.) Franco	164	(35 %)	28.04	(67 %)	2 %	35.9
	<i>Quercus robur</i> L.	5	(1 %)	2.40	(6 %)	0 %	27.8
	<i>Sambucus nigra</i> L.	8	(2 %)	0.02	(0 %)	0 %	6.4
	<i>Sorbus torminalis</i> (L.) Crantz	1	(0 %)	0.01	(0 %)	0 %	13.3
	<i>Taxus baccata</i> L.	18	(4 %)	0.89	(2 %)	33 %	6.2
	<i>Tilia spec.</i> L.	9	(2 %)	0.46	(1 %)	11 %	16.9
	<i>Tsuga heterophylla</i> (Raf.) Sarg.	3	(1 %)	0.43	(1 %)	0 %	20.8
	unidentified broad-leaved	4	(1 %)	0.05	(0 %)	100 %	13.8
BR05	all	331	(100 %)	33.28	(100 %)	5 %	26.6
	<i>Betula pendula</i> Roth	2	(1 %)	0.03	(0 %)	0 %	11.4
	<i>Carpinus betulus</i> L.	17	(5 %)	0.96	(3 %)	0 %	17.2
	<i>Fagus sylvatica</i> L.	148	(45 %)	12.15	(37 %)	5 %	23.7
	<i>Juglans regia</i> L.	32	(10 %)	0.71	(2 %)	3 %	15.8
	<i>Larix decidua</i> Mill.	21	(6 %)	4.10	(12 %)	0 %	31.5
	<i>Picea abies</i> (L.) H. Karst.	42	(13 %)	3.45	(10 %)	5 %	28.6
	<i>Pinus sylvestris</i> L.	6	(2 %)	1.56	(5 %)	33 %	36.1
	<i>Pseudotsuga menziesii</i> (Mirb.) Franco	44	(13 %)	7.42	(22 %)	2 %	37.7
	<i>Quercus petraea</i> (Matt.) Franco	17	(5 %)	2.86	(9 %)	0 %	33.7
	<i>Salix caprea</i> L.	1	(0 %)	0.03	(0 %)	0 %	18.4
	unidentified coniferous	1	(0 %)	0.01	(0 %)	100 %	9.3

Table A1. Continued.

Plot	Species	No. of trees		Basal area [m ² ha ⁻¹]		Percentage of dead trees	Median height [m]
		abs.	rel.	abs.	rel.		
KA09	all	272	(100 %)	25.21	(100 %)	8 %	20.2
	<i>Acer pseudoplatanus</i> L.	1	(0 %)	0.01	(0 %)	0 %	10.3
	<i>Amelanchier lamarckii</i> (Raf.) F. G. Schroed.	3	(1 %)	0.01	(0 %)	0 %	10.0
	<i>Betula pendula</i> Roth	17	(6 %)	0.16	(1 %)	0 %	11.8
	<i>Carpinus betulus</i> L.	17	(6 %)	0.08	(0 %)	0 %	7.2
	<i>Castanea sativa</i> Mill.	2	(1 %)	0.01	(0 %)	0 %	7.0
	<i>Fagus sylvatica</i> L.	101	(37 %)	7.68	(30 %)	0 %	20.5
	<i>Ilex aquifolium</i> L.	5	(2 %)	0.02	(0 %)	0 %	5.6
	<i>Picea abies</i> (L.) H. Karst.	32	(12 %)	3.20	(13 %)	50 %	24.4
	<i>Pinus sylvestris</i> L.	64	(24 %)	13.32	(53 %)	2 %	30.7
	<i>Populus tremula</i> L.	1	(0 %)	0.01	(0 %)	0 %	10.8
	<i>Prunus avium</i> (L.) L.	5	(2 %)	0.02	(0 %)	20 %	7.1
	<i>Quercus rubra</i> L.	13	(5 %)	0.65	(3 %)	0 %	11.6
	<i>Sambucus nigra</i> L.	5	(2 %)	0.03	(0 %)	40 %	4.4
	<i>Sorbus aucuparia</i> L.	3	(1 %)	0.01	(0 %)	0 %	7.4
	<i>Taxus baccata</i> L.	1	(0 %)	0.00	(0 %)	0 %	3.8
	unidentified broad-leaved	2	(1 %)	0.00	(0 %)	100 %	6.3
KA10	all	426	(100 %)	23.06	(100 %)	3 %	11.7
	<i>Acer pseudoplatanus</i> L.	28	(7 %)	0.27	(1 %)	0 %	10.1
	<i>Aesculus hippocastanum</i> L.	1	(0 %)	0.26	(1 %)	0 %	17.3
	<i>Betula pendula</i> Roth	2	(0 %)	0.16	(1 %)	0 %	19.7
	<i>Carpinus betulus</i> L.	108	(25 %)	3.82	(17 %)	4 %	15.1
	<i>Castanea sativa</i> Mill.	11	(3 %)	0.15	(1 %)	0 %	11.6
	<i>Ilex aquifolium</i> L.	7	(2 %)	0.04	(0 %)	0 %	9.0
	<i>Pinus sylvestris</i> L.	27	(6 %)	5.02	(22 %)	7 %	26.7
	<i>Prunus serotina</i> Ehrh., nom. cons.	140	(33 %)	0.88	(4 %)	1 %	7.0
	<i>Quercus rubra</i> L.	91	(21 %)	12.30	(53 %)	0 %	23.6
	<i>Robinia pseudoacacia</i> L.	3	(1 %)	0.07	(0 %)	0 %	14.2
	<i>Sambucus nigra</i> L.	4	(1 %)	0.04	(0 %)	75 %	6.2
	<i>Tilia spec.</i> L.	3	(1 %)	0.03	(0 %)	0 %	8.9
	unidentified broad-leaved	1	(0 %)	0.02	(0 %)	100 %	14.5
KA11	all	787	(100 %)	28.66	(100 %)	3 %	15.7
	<i>Acer pseudoplatanus</i> L.	4	(1 %)	0.02	(0 %)	0 %	10.4
	<i>Fagus sylvatica</i> L.	309	(39 %)	3.65	(13 %)	4 %	12.2
	<i>Picea abies</i> (L.) H. Karst.	10	(1 %)	0.20	(1 %)	50 %	10.6
	<i>Pinus sylvestris</i> L.	98	(12 %)	10.62	(37 %)	1 %	24.8
	<i>Prunus serotina</i> Ehrh., nom. cons.	118	(15 %)	1.26	(4 %)	4 %	9.4
	<i>Pseudotsuga menziesii</i> (Mirb.) Franco	5	(1 %)	0.29	(1 %)	20 %	29.3
	<i>Quercus petraea</i> (Matt.) Liebl.	18	(2 %)	0.71	(2 %)	0 %	17.9
	<i>Quercus rubra</i> L.	219	(28 %)	11.82	(41 %)	0 %	22.3
	<i>Tilia spec.</i> L.	5	(1 %)	0.09	(0 %)	0 %	12.0
	unidentified broad-leaved	1	(0 %)	0.00	(0 %)	100 %	9.0

Supplement. The supplement related to this article is available online at: <https://doi.org/10.5194/essd-14-2989-2022-supplement>.

Author contributions. BH and FEF conceived the study. LW, JS, NK and HW collected and analyzed the data. FEF, JS and HW drafted the manuscript. All authors reviewed the manuscript.

Competing interests. The contact author has declared that none of the authors has any competing interests.

Disclaimer. Publisher's note: Copernicus Publications remains neutral with regard to jurisdictional claims in published maps and institutional affiliations.

Acknowledgements. We acknowledge Christian Seitz, Marian Schimka, Katharina Anders, Paula Kuss, Veit Ulrich, Vivien Zahs, Felix Schiefer, Elham Shafeian, Denis Debroize, Annika Denner, Michael Ewald, Lioba Martin, Helen Hake, Tobias Steinert, Vanessa Rittlinger, Fabio Bothner, Louisa Lücking, Janina Schüssler, Angelo Mayer, Katharina Ruge, Johannes Brand, Lea Schraml, Naia Haltmeier, Carolin Klonner, Daria Baete, Thorben Schrempp, Lisa-Maricia Schwarz and Andressa Soarez Braz for their assistance with data acquisition and processing.

Financial support. This research has been supported by the Deutsche Forschungsgemeinschaft (grant no. 411263134).

Review statement. This paper was edited by Sibylle K. Hassler and reviewed by Louise Terryn and one anonymous referee.

References

- Applanix Corporation: POSPAC MMS 8, https://www.applanix.com/downloads/products/specs/POSPac_MMS_8_Infosheet.pdf (last access: 24 June 2022), 2018.
- Arumäe, T. and Lang, M.: Estimation of Canopy Cover in Dense Mixed-Species Forests Using Airborne Lidar Data, *Eur. J. Remote Sens.*, 51, 132–141, <https://doi.org/10.1080/22797254.2017.1411169>, 2018.
- ASPRS: LAS Specification Version 1.2, http://www.asprs.org/a/society/committees/standards/asprs_las_format_v12.pdf (last access: 27 July 2021), 2008.
- ASPRS: LAS Specification Version 1.4 – R13, https://www.asprs.org/a/society/committees/standards/LAS_1_4_r13.pdf (last access: 27 July 2021), 2013.
- Barber, C. B., Dobkin, D. P., and Huhdanpaa, H.: The Quickhull algorithm for convex hulls, *ACM T. Math. Software*, 22, 469–483, 1996.
- Boudon, F.: PlantScan3D, GitHub [code], <https://github.com/fredboudon/plantscan3d> (last access: 24 June 2022), 2021.
- Bournez, E., Landes, T., Saudreau, M., Kastendeuch, P., and Najar, G.: From TLS Point Clouds to 3D Models of Trees: a Comparison of Existing Algorithms for 3D Tree Reconstruction, *Int. Arch. Photogramm. Remote Sens. Spatial Inf. Sci.*, XLII-2/W3, 113–120, <https://doi.org/10.5194/isprs-archives-XLII-2-W3-113-2017>, 2017.
- Bouvier, M., Durrieu, S., Fournier, R. A., and Renaud, J.-P.: Generalizing Predictive Models of Forest Inventory Attributes Using an Area-Based Approach with Airborne LiDAR Data, *Remote Sens. Environ.*, 156, 322–334, <https://doi.org/10.1016/j.rse.2014.10.004>, 2015.
- Bruggisser, M., Hollaus, M., Otepka, J., and Pfeifer, N.: Influence of ULS acquisition characteristics on tree stem parameter estimation, *ISPRS J. Photogramm.*, 168, 28–40, <https://doi.org/10.1016/j.isprsjprs.2020.08.002>, 2020.
- Calders, K., Lewis, P., Disney, M., Verbesselt, J., and Herold, M.: Investigating assumptions of crown archetypes for modelling LiDAR returns, *Remote Sens. Environ.*, 134, 39–49, <https://doi.org/10.1016/j.rse.2013.02.018>, 2013.
- Calders, K., Newnham, G., Burt, A., Murphy, S., Raumonen, P., Herold, M., Culvenor, D., Avitabile, V., Disney, M., Armston, J., and Kaasalainen, M.: Nondestructive estimates of above-ground biomass using terrestrial laser scanning, *Methods Ecol. Evol.*, 6, 198–208, <https://doi.org/10.1111/2041-210X.12301>, 2015.
- Calders, K., Adams, J., Armston, J., Bartholomeus, H., Bauwens, S., Bentley, L. P., Chave, J., Danson, F. M., Demol, M., Disney, M., Gaulton, R., Krishna Moorthy, S. M., Levick, S. R., Saarinen, N., Schaaf, C., Stovall, A., Terryn, L., Wilkes, P., and Verbeeck, H.: Terrestrial laser scanning in forest ecology: Expanding the horizon, *Remote Sens. Environ.*, 251, 112102, <https://doi.org/10.1016/j.rse.2020.112102>, 2020.
- CloudCompare: CloudCompare, version 2.10.2, GitHub [code], <https://github.com/CloudCompare/CloudCompare/releases/tag/v2.10.2>, last access: 3 April 2019.
- Computree Group: Computree, http://computree.onf.fr/?page_id=589, last access: 24 June 2022.
- Craig, A.: The Concave Hull of a Set of Points, Code-Project [code], <https://www.codeproject.com/Articles/1201438/The-Concave-Hull-of-a-Set-of-Points> (last access: 1 December 2020), 2017.
- Dassot, M., Colin, A., Santenoise, P., Fournier, M., and Constant, T.: Terrestrial laser scanning for measuring the solid wood volume, including branches, of adult standing trees in the forest environment, *Comput. Electron. Agr.*, 89, 86–93, <https://doi.org/10.1016/j.compag.2012.08.005>, 2012.
- Disney, M. I., Kalogirou, V., Lewis, P., Prieto-Blanco, A., Hancock, S., and Pfeifer, M.: Simulating the impact of discrete-return lidar system and survey characteristics over young conifer and broadleaf forests, *Remote Sens. Environ.*, 114, 1546–1560, <https://doi.org/10.1016/j.rse.2010.02.009>, 2010.
- Disney, M. I., Boni Vicari, M., Burt, A., Calders, K., Lewis, S. L., Raumonen, P., and Wilkes, P.: Weighing trees with lasers: advances, challenges and opportunities, *Interface Focus*, 8, 20170048, <https://doi.org/10.1098/rsfs.2017.0048>, 2018.
- DJI: MATRICE 600 PRO – User Manual, https://dl.djicdn.com/downloads/m600pro/1208EN/Matrice_600_Pro_User_Manual_v1.0_EN_1208.pdf (last access: 17 May 2021), 2018.
- Du, S., Lindenbergh, R., Ledoux, H., Stoter, J., and Nan, L.: AdTree: Accurate, Detailed, and Automatic Mod-

- elling of Laser-Scanned Trees, *Remote Sensing*, 11, 2074, <https://doi.org/10.3390/rs11182074>, 2019.
- Dubayah, R., Blair, J. B., Goetz, S., Fatoyinbo, L., Hansen, M., Healey, S., Hofton, M., Hurt, G., Kellner, J., Luthcke, S., Armston, J., Tang, H., Duncanson, L., Hancock, S., Jantz, P., Marselis, S., Patterson, P. L., Qi, W., and Silva, C.: The Global Ecosystem Dynamics Investigation: High-resolution laser ranging of the Earth's forests and topography, *Sci. Remote Sens.*, 1, 100002, <https://doi.org/10.1016/j.srs.2020.100002>, 2020.
- Fu, H., Li, H., Dong, Y., Xu, F., and Chen, F.: Segmenting Individual Tree from TLS Point Clouds Using Improved DBSCAN, *Forests*, 13, 566, <https://doi.org/10.3390/f13040566>, 2022.
- Gastellu-Etchegorry, J. P., Martin, E., and Gascon, F.: DART: a 3D model for simulating satellite images and studying surface radiation budget, *Int. J. Remote Sens.*, 25, 73–96, <https://doi.org/10.1080/0143116031000115166>, 2004.
- Gastellu-Etchegorry, J.-P., Yin, T., Lauret, N., Cajgfinger, T., Greigoire, T., Grau, E., Feret, J.-B., Lopes, M., Guilleux, J., Dedieu, G., Malenovský, Z., Cook, B. D., Morton, D., Rubio, J., Durrieu, S., Cazanave, G., Martin, E., and Ristorcelli, T.: Discrete Anisotropic Radiative Transfer (DART 5) for Modeling Airborne and Satellite Spectroradiometer and LIDAR Acquisitions of Natural and Urban Landscapes, *Remote Sensing*, 7, 1667–1701, <https://doi.org/10.3390/rs70201667>, 2015.
- Hackenberg, J.: SimpleTree Plugin, version Beta 4.33.06, <https://rdinnovation.onfr/projects/computree-simplenet-beta-version/files> (last access: 21 May 2019), 2017.
- Hackenberg, J.: SimpleForest: A tree modelling software, <https://simpleforest.org/> (last access: 24 June 2022), 2021.
- Hackenberg, J., Spiecker, H., Calders, K., Disney, M., and Rauomonen, P.: SimpleTree – An Efficient Open Source Tool to Build Tree Models from TLS Clouds, *Forests*, 6, 4245–4294, <https://doi.org/10.3390/f6114245>, 2015.
- Höfle, B., Qu, J., Winiwarter, L., Weiser, H., Zahs, V., Schäfer, J., and Fassnacht, F. E.: pytreeDB: library for point clouds of tree vegetation objects, GitHub [code], <https://github.com/3dgeo-heidelberg/pytreeDB>, last access: 24 June 2022.
- Holopainen, M., Vastaranta, M., and Hyppä, J.: Outlook for the Next Generation's Precision Forestry in Finland, *Forests*, 5, 1682–1694, <https://doi.org/10.3390/f5071682>, 2014.
- Krishna Moorthy, S. M., Calders, K., Vicari, M. B., and Verbeeck, H.: Improved Supervised Learning-Based Approach for Leaf and Wood Classification From LiDAR Point Clouds of Forests, *IEEE T. Geosci. Remote Sens.*, 58, 3057–3070, <https://doi.org/10.1109/TGRS.2019.2947198>, 2020.
- Latifi, H., Fassnacht, F. E., Müller, J., Tharani, A., Dech, S., and Heurich, M.: Forest inventories by LiDAR data: A comparison of single tree segmentation and metric-based methods for inventories of a heterogeneous temperate forest, *Int. J. Appl. Earth Obs.*, 42, 162–174, <https://doi.org/10.1016/j.jag.2015.06.008>, 2015.
- Lewis, P.: Three-dimensional plant modelling for remote sensing simulation studies using the Botanical Plant Modelling System, *Agronomie*, 19, 185–210, <https://doi.org/10.1051/agro:19990302>, 1999.
- Lewis, P. and Muller, J.-P.: The Advanced Radiometric Ray-Tracer (ARARAT) for plant canopy reflectance simulation, *Int. Arch. Photogramm. Rem. Sens.*, (Commission VII(B7)) 29, 26–34, https://www.isprs.org/proceedings/XXIX/congress/part7/26_XXIX-part7.pdf (last access: 24 June 2022), 1992.
- Liu, G., Wang, J., Dong, P., Chen, Y., and Liu, Z.: Estimating Individual Tree Height and Diameter at Breast Height (DBH) from Terrestrial Laser Scanning (TLS) Data at Plot Level, *Forests*, 9, 398, <https://doi.org/10.3390/f9070398>, 2018.
- Maltamo, M., Eerikäinen, K., Pitkänen, J., Hyppä, J., and Vehmas, M.: Estimation of timber volume and stem density based on scanning laser altimetry and expected tree size distribution functions, *Remote Sens. Environ.*, 90, 319–330, <https://doi.org/10.1016/j.rse.2004.01.006>, 2004.
- Maltamo, M., Næsset, E., and Vauhkonen, J. (Eds.): *Forestry Applications of Airborne Laser Scanning*, Vol. 27, Springer Netherlands, Dordrecht, ISBN 978-94-017-8663-8, 2014.
- Montaghi, A., Corona, P., Dalponte, M., Gianelle, D., Chirici, G., and Olsson, H.: Airborne laser scanning of forest resources: An overview of research in Italy as a commentary case study, *Int. J. Appl. Earth Obs.*, 23, 288–300, <https://doi.org/10.1016/j.jag.2012.10.002>, 2013.
- Moreira, A. and Yasmina Santos, M.: Concave hull: A k -nearest neighbours approach for the computation of the region occupied by a set of points, in: *Proceedings of the Second International Conference on Computer Graphics Theory and Applications – Volume 2: GRAPP*, 61–68, INSTICC, SciTePress, <https://doi.org/10.5220/0002080800610068>, 2007.
- Morsdorf, F., Eck, C., Zgraggen, C., Imbach, B., Schneider, F. D., and Kükenbrink, D.: UAV-based LiDAR acquisition for the derivation of high-resolution forest and ground information, *Leading Edge*, 36, 566–570, <https://doi.org/10.1190/tle36070566.1>, 2017.
- Nan, L., Messal, L., Du, S., and Yang, Z.: AdTree, GitHub [code], <https://github.com/tudelft3d/adtree> (last access: 24 June 2022), 2021.
- Næsset, E.: Predicting Forest Stand Characteristics with Airborne Scanning Laser Using a Practical Two-Stage Procedure and Field Data, *Remote Sens. Environ.*, 80, 88–99, [https://doi.org/10.1016/S0034-4257\(01\)00290-5](https://doi.org/10.1016/S0034-4257(01)00290-5), 2002.
- Næsset, E., Gobakken, T., Solberg, S., Greigoire, T. G., Nelson, R., Ståhl, G., and Weydahl, D.: Model-Assisted Regional Forest Biomass Estimation Using LiDAR and InSAR as Auxiliary Data: A Case Study from a Boreal Forest Area, *Remote Sens. Environ.*, 115, 3599–3614, <https://doi.org/10.1016/j.rse.2011.08.021>, 2011.
- Pearse, G. D., Watt, M. S., Dash, J. P., Stone, C., and Caccamo, G.: Comparison of Models Describing Forest Inventory Attributes Using Standard and Voxel-Based Lidar Predictors across a Range of Pulse Densities, *Int. J. Appl. Earth Obs.*, 78, 341–351, <https://doi.org/10.1016/j.jag.2018.10.008>, 2019.
- Pfeifer, N., Mandlburger, G., Otepka, J., and Karel, W.: OPALS – A framework for Airborne Laser Scanning data analysis, *Comput. Environ. Urban*, 45, 125–136, <https://doi.org/10.1016/j.compenvurbsys.2013.11.002>, 2014.
- Pfennigbauer, M. and Ullrich, A.: Improving quality of laser scanning data acquisition through calibrated amplitude and pulse deviation measurement, in: *Laser Radar Technology and Applications XV*, edited by: Turner, M. D. and Kamerman, G. W., Vol. 7684, 463–472, International Society for Optics and Photonics, SPIE, <https://doi.org/10.1117/12.849641>, 2010.
- Rapidlasso GmbH: LAStools – efficient LiDAR processing software (version 200509, unlicensed), <https://rapidlasso.com/las-tools/>, last access: 9 June 2020.

- Raumonen, P.: TreeQSM: Reconstruction of quantitative structure models of trees from point cloud data, Zenodo [code], <https://doi.org/10.5281/zenodo.844625>, 2020.
- Raumonen, P., Kaasalainen, M., Åkerblom, M., Kaasalainen, S., Kaartinen, H., Vastaranta, M., Holopainen, M., Disney, M., and Lewis, P.: Fast Automatic Precision Tree Models from Terrestrial Laser Scanner Data, *Remote Sens.*, 5, 491–520, <https://doi.org/10.3390/rs5020491>, 2013.
- RIEGL* Laser Measurement Systems: *RIEGL* VZ-400, Data Sheet, https://download.pangaea.de/reference/109168/attachments/10_DataSheet_VZ-400_2017-06-14.pdf (last access: 10 June 2022), 2017.
- RIEGL* Laser Measurement Systems: *RIEGL* VQ-780i, Data Sheet, https://download.pangaea.de/reference/109170/attachments/RIEGL_VQ-780i_Datasheet_2019-09-02.pdf (last access: 10 June 2021), 2019.
- RIEGL* Laser Measurement Systems: Data Processing Software RiPROCESS for *RIEGL* Scan Data, http://www.riegl.com/uploads/tx_pxpriegldownloads/RiProcess_Datasheet_2020-08-20_01.pdf (last access: 23 March 2021), 2020a.
- RIEGL* Laser Measurement Systems: Operating & Processing Software RiSCAN PRO for *RIEGL* 3D Laser Scanners, http://www.riegl.com/uploads/tx_pxpriegldownloads/RiSCAN-PRO_DataSheet_2020-10-07.pdf (last access: 4 July 2022), 2020b.
- RIEGL* Laser Measurement Systems: *RIEGL* miniVUX-1UAV, Data Sheet, https://download.pangaea.de/reference/109169/attachments/RIEGL_miniVUX-1UAV_Datasheet_2020-10-06.pdf (last access: 10 June 2022), 2020c.
- Roberts, O., Bunting, P., Hardy, A., and McInerney, D.: Sensitivity Analysis of the DART Model for Forest Mensuration with Airborne Laser Scanning, *Remote Sens.*, 12, 247, <https://doi.org/10.3390/rs12020247>, 2020.
- Roussel, J.-R., Auty, D., Coops, N. C., Tompalski, P., Goodbody, T. R., Meador, A. S., Bourdon, J.-F., de Boissieu, F., and Achim, A.: lidR: An R package for analysis of Airborne Laser Scanning (ALS) data, *Remote Sens. Environ.*, 251, 112061, <https://doi.org/10.1016/j.rse.2020.112061>, 2020.
- Rusu, R. B. and Cousins, S.: 3D is here: Point Cloud Library (PCL), in: IEEE International Conference on Robotics and Automation (ICRA), Shanghai, China, <https://doi.org/10.1109/ICRA.2011.5980567>, 2011.
- Rusu, R. B., Marton, Z. C., Blodow, N., Dolha, M., and Beetz, M.: Towards 3D Point cloud based object maps for household environments, *Robot. Auton. Syst.*, 56, 927–941, <https://doi.org/10.1016/j.robot.2008.08.005>, 2008.
- Scion: Forest Science, Brochure, https://www.scionresearch.com/_data/assets/pdf_file/0003/51645/Forest_Science_Brochure.pdf (last access: 25 April 2022), 2021.
- Sinoquet, H., Le Roux, X., Adam, B., Ameglio, T., and Daudet, F. A.: RATP: a model for simulating the spatial distribution of radiation absorption, transpiration and photosynthesis within canopies: application to an isolated tree crown, *Plant Cell Environ.*, 24, 395–406, <https://doi.org/10.1046/j.1365-3040.2001.00694.x>, 2001.
- Smith, A. M. S., Falkowski, M. J., Hudak, A. T., Evans, J. S., Robinson, A. P., and Steele, C. M.: A Cross-Comparison of Field, Spec-
tral, and Lidar Estimates of Forest Canopy Cover, *Can. J. Remote Sens.*, 35, 447–459, <https://doi.org/10.5589/m09-038>, 2009.
- Vicari, M. B.: TLSeparation, GitHub [code], <https://github.com/TLSeparation> (last access: 24 June 2022), 2021.
- Vicari, M. B., Disney, M., Wilkes, P., Burt, A., Calders, K., and Woodgate, W.: Leaf and wood classification framework for terrestrial LiDAR point clouds, *Methods Ecol. Evol.*, 10, 680–694, <https://doi.org/10.1111/2041-210X.13144>, 2019.
- Vincent, G., Antin, C., Laurans, M., Heurtebize, J., Durrieu, S., Lavallee, C., and Dauzat, J.: Mapping plant area index of tropical evergreen forest by airborne laser scanning. A cross-validation study using LAI2200 optical sensor, *Remote Sens. Environ.*, 198, 254–266, <https://doi.org/10.1016/j.rse.2017.05.034>, 2017.
- Wallace, L., Musk, R., and Lucieer, A.: An Assessment of the Repeatability of Automatic Forest Inventory Metrics Derived From UAV-Borne Laser Scanning Data, *IEEE T. Geosci. Remote Sens.*, 52, 7160–7169, <https://doi.org/10.1109/TGRS.2014.2308208>, 2014.
- Wang, D.: LeWoS, Zenodo [code], <https://doi.org/10.5281/zenodo.3516856>, 2020.
- Wang, D., Momo Takoudjou, S., and Casella, E.: LeWoS: A universal leaf-wood classification method to facilitate the 3D modelling of large tropical trees using terrestrial LiDAR, *Methods Ecol. Evol.*, 11, 376–389, <https://doi.org/10.1111/2041-210X.13342>, 2020.
- Wang, Y., Lehtomäki, M., Liang, X., Pyörälä, J., Kukko, A., Jaakkola, A., Liu, J., Feng, Z., Chen, R., and Hyppä, J.: Is field-measured tree height as reliable as believed – A comparison study of tree height estimates from field measurement, airborne laser scanning and terrestrial laser scanning in a boreal forest, *ISPRS J. Photogramm.*, 147, 132–145, <https://doi.org/10.1016/j.isprsjprs.2018.11.008>, 2019.
- Weiser, H.: 3dgeo-heidelberg/syssifoss: Version 1.0.0, Zenodo [code], <https://doi.org/10.5281/zenodo.6759913>, 2022.
- Weiser, H., Winiwarter, L., Anders, K., Fassnacht, F. E., and Höfle, B.: Opaque voxel-based tree models for virtual laser scanning in forestry applications, *Remote Sens. Environ.*, 265, 112641, <https://doi.org/10.1016/j.rse.2021.112641>, 2021.
- Weiser, H., Schäfer, J., Winiwarter, L., Krašovec, N., Seitz, C., Schimka, M., Anders, K., Baete, D., Braz, A. S., Brand, J., Debroize, D., Kuss, P., Martin, L. L., Mayer, A., Schrempp, T., Schwarz, L.-M., Ulrich, V., Fassnacht, F. E., and Höfle, B.: Terrestrial, UAV-borne, and airborne laser scanning point clouds of central European forest plots, Germany, with extracted individual trees and manual forest inventory measurements, PANGAEA [data set], <https://doi.org/10.1594/PANGAEA.942856>, 2022a.
- Weiser, H., Schäfer, J., Winiwarter, L., Krašovec, N., Seitz, C., Schimka, M., Anders, K., Baete, D., Braz, A. S., Brand, J., Debroize, D., Kuss, P., Martin, L. L., Mayer, A., Schrempp, T., Schwarz, L.-M., Ulrich, V., Fassnacht, F. E., and Höfle, B.: Terrestrial, UAV-borne, and airborne laser scanning point clouds of central European forest plots, Germany, with extracted individual trees and manual forest inventory measurements – Metadata Documentation, https://download.pangaea.de/reference/109167/attachments/SYSSIFOSS_2019-2020_meta_4.pdf (last access: 24 June 2022), 2022b.
- White, J. C., Tompalski, P., Vastaranta, M., Wulder, M. A., Saarenen, N., Stepper, C., and Coops, N. C.: A model development and application guide for generating an enhanced forest in-

- ventory using airborne laser scanning data and an area-based approach, CWFC Information Report FI-X-018, Natural Resources Canada, Victoria, BC, Canada, <https://cfs.nrcan.gc.ca/pubwarehouse/pdfs/38945.pdf> (last access: 24 June 2022), 2017.
- Widlowski, J.-L., Lavergne, T., Pinty, B., Verstraete, M., and Gobron, N.: Rayspread: A Virtual Laboratory for Rapid BRF Simulations Over 3-D Plant Canopies, in: Computational Methods in Transport, edited by: Graziani, F., 211–231, Springer, Berlin, Heidelberg, 211–231, https://doi.org/10.1007/3-540-28125-8_10, 2006.
- Widlowski, J.-L., Mio, C., Disney, M., Adams, J., Andredakis, I., Atzberger, C., Brennan, J., Busetto, L., Chelle, M., Ceccherini, G., Colombo, R., Côté, J.-F., Eenmäe, A., Essery, R., Gastellu-Etchegorry, J.-P., Gobron, N., Grau, E., Haverd, V., Homolová, L., Huang, H., Hunt, L., Kobayashi, H., Koetz, B., Kuusk, A., Kuusk, J., Lang, M., Lewis, P. E., Lovell, J. L., Malenovský, Z., Meroni, M., Morsdorf, F., Möttus, M., Ni-Meister, W., Pinty, B., Rautainen, M., Schlerf, M., Somers, B., Stuckens, J., Verstraete, M. M., Yang, W., Zhao, F., and Zenone, T.: The fourth phase of the radiative transfer model intercomparison (RAMI) exercise: Actual canopy scenarios and conformity testing, *Remote Sens. Environ.*, 169, 418–437, <https://doi.org/10.1016/j.rse.2015.08.016>, 2015.
- Winiwarter, L., Pena, A. M. E., Weiser, H., Anders, K., Sanches, J. M., Searle, M., and Höfle, B.: 3dgeo-heidelberg/helios, Zenodo [code], <https://doi.org/10.5281/zenodo.4452870>, 2021.
- Winiwarter, L., Esmorís Pena, A. M., Weiser, H., Anders, K., Martínez Sánchez, J., Searle, M., and Höfle, B.: Virtual laser scanning with HELIOS++: A novel take on ray tracing-based simulation of topographic full-waveform 3D laser scanning, *Remote Sens. Environ.*, 269, 112772, <https://doi.org/10.1016/j.rse.2021.112772>, 2022.
- Yun, T., An, F., Li, W., Sun, Y., Cao, L., and Xue, L.: A Novel Approach for Retrieving Tree Leaf Area from Ground-Based LiDAR, *Remote Sens.*, 8, 942, <https://doi.org/10.3390/rs8110942>, 2016.
- Zhou, J., Wei, H., Zhou, G., and Song, L.: Separating Leaf and Wood Points in Terrestrial Laser Scanning Data Using Multiple Optimal Scales, *Sensors*, 19, 1852, <https://doi.org/10.3390/s19081852>, 2019.